

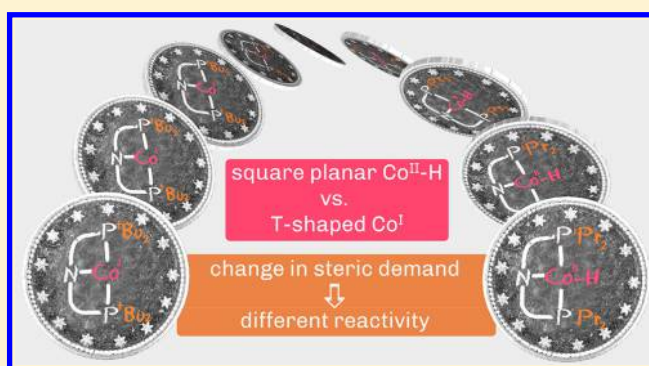
Square Planar Cobalt(II) Hydride versus T-Shaped Cobalt(I): Structural Characterization and Dihydrogen Activation with PNP–Cobalt Pincer Complexes

Lukas S. Merz, Clemens K. Blasius, Hubert Wadepohl, and Lutz H. Gade*[✉]

Anorganisch Chemisches Institut, Universität Heidelberg, Im Neuenheimer Feld 270, Heidelberg 69120, Germany

Supporting Information

ABSTRACT: The carbazole-based pincer ligand $R(\text{CbzPNP})\text{H}$ ($R = \text{Pr}, \text{Bu}$) has been used for the synthesis and characterization of various low- and high-spin cobalt complexes. Upon treatment of the high-spin complexes $R(\text{CbzPNP})\text{CoCl}$ ($2^R\text{-Co}^{\text{II}}\text{Cl}$) with NaHBET_3 , the selective formation of cobalt(II) hydride $3^{\text{Pr}}\text{-Co}^{\text{II}}\text{H}$ and T-shaped cobalt(I) complex $4^{\text{Bu}}\text{-Co}^{\text{I}}$ was observed, depending on the substituents at the phosphorus atoms. For an unambiguous characterization of the reaction products, a density functional theory (DFT) supported paramagnetic NMR analysis was carried out, which established the electron configuration and the oxidation states of the metal atoms, thus demonstrating the significant impact of ligand substitution on the outcome of the reaction. A distinct one-electron reactivity was found for $4^{\text{Bu}}\text{-Co}^{\text{I}}$ in the dehalogenation of tBuCl and cleavage of PhSSPh . On the other hand, the Co^{I} species displayed two-electron redox behavior in the oxidative addition of dihydrogen. The resulting dihydride complex $6^{\text{Bu}}\text{-Co}^{\text{III}}(\text{H})_2$ was found to display sluggish reactivity toward alkenes, whereas the cobalt(II) hydride $3^{\text{Pr}}\text{-Co}^{\text{II}}\text{H}$ was successfully employed in the catalytic hydrogenation of unhindered alkenes. The stoichiometric hydrogenolysis of $8^{\text{Pr}}\text{-Co}^{\text{II}}\text{Bn}$ at elevated pressure (10 bar) led to a rapid cleavage of the $\text{Co}-\text{C}$ bond to yield hydride complex $3^{\text{Pr}}\text{-Co}^{\text{II}}\text{H}$. On the other hand, treatment of $2^{\text{Pr}}\text{-Co}^{\text{II}}\text{Cl}$ with phenethylmagnesium chloride directly resulted in the formation of $3^{\text{Pr}}\text{-Co}^{\text{II}}\text{H}$, indicating facile $\beta\text{-H}$ elimination of the alkene insertion product (reversibly) generated in the catalytic hydrogenation. On the basis of these observations, a mechanistic pathway involving a key σ -bond metathesis step of the Co^{II} -alkyl species is proposed.



INTRODUCTION

As part of the rapid development of base metal catalysis during the past two decades, first-row transition metal pincer complexes have acquired a privileged status. Their application in catalytic transformations has focused primarily on coupling reactions as well as reductions.¹ For the latter, catalytic hydrogenations and their reverse reactions are of particular interest. A notable contrast to the reaction patterns encountered in noble metal catalysis is the accessibility of multiple spin states as well as the tendency to favor one-electron redox processes.²

As for the other 3d metals, the open shell electron configuration as well as the tendency toward single electron redox chemistry of cobalt give rise to specific challenges in the exploitation of its catalytic reactivity.³ Nevertheless, various cobalt catalyzed transformations, such as (de)hydrogenations,⁴ hydrosilylations/-borylations^{2d,5} and C–H functionalizations⁶ have been reported recently. The precatalysts employed in such reactions can basically be divided into two classes: (i) mainly carbonyl-supported 16 or 18 valence electron *low-spin* complexes and (ii) coordinatively unsaturated *high-spin* (pre)catalysts.⁷ For the latter, halide or alkyl complexes prevail

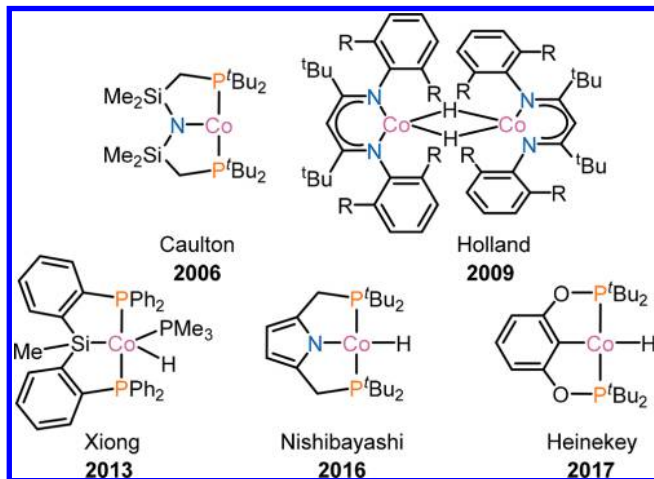
as precatalysts due to their facile conversion into the corresponding hydride systems, which have been identified in several mechanistic investigations as fundamental intermediates in reduction catalysis.^{4a,b,6a,c,8} However, there are but a few examples of isolated $\text{Co}^{\text{II}}\text{-H}$ complexes, contrasting the greater number of reports on Co^{I} hydrides.⁹

To our knowledge, only a few pincer ligand-supported Co^{II} hydride complexes have been isolated to date (Chart 1),¹⁰ which in part may be due to the propensity of Co^{II} alkyl and hydride complexes to undergo one-electron reduction to form the corresponding Co^{I} complexes. Most recently, this was demonstrated by Tonzetich and co-workers, when they attempted to resynthesize the previously reported pyrrole-based (PNP) $\text{Co}^{\text{II}}\text{-H}$ complex (Chart 1, center bottom).^{10c,d,11}

Nevertheless, the direct isolation of the primary one-electron reduction products from Co^{II} alkyl and hydride complexes appears to be challenging despite their propensity for this type of transformation. The isolation of Co^{I} complexes normally requires additional donor ligands, resulting in more highly

Received: February 9, 2019

Chart 1. Selection of Fully Characterized Pincer Type Co^{II} Hydride Complexes As Well As the Only Known T-Shaped Co^I Complex



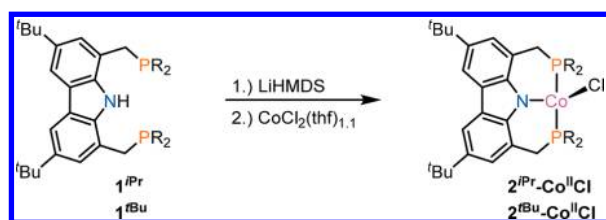
coordinated products.^{9d,10d,11,12} Thus, pincer type Co^I complexes have been isolated as square planar molecules with additional dinitrogen or carbon monoxide ligands in the coordination plane.^{10d,11,12a,c} Accordingly, there have been only few reports on T-shaped Co^I pincer complexes, the most notable example being Caulton's PNPCo^I compound reported more than a decade ago (Chart 1).^{2a,13}

We recently reported a carbazole-based PNP pincer ligand, R(C^{cbz}PNP)H, which has been used in a series of synthetic and mechanistic studies involving both early and late transition metals.¹⁴ In particular, the stabilization of a variety of reactive transition metal hydrido complexes has been achieved.^{14a,b,15} Given the burgeoning interest in the field of reduction catalysis involving cobalt pincer compounds, we envisioned that this carbazole-derived PNP ligand could confer sufficient stability upon low-coordinate Co^{II} hydrides, as well as related species, to allow for their convenient synthesis and a first investigation into their reactivity.

RESULTS AND DISCUSSION

The R(C^{cbz}PNP) protio-ligands ⁱPr(C^{cbz}PNP)H and ^tBu(C^{cbz}PNP)H were prepared according to previously reported procedures.^{14c,16} Upon lithiation with LiHMDS (lithium hexamethyldisilazide), both ligands were reacted with [CoCl₂(thf)_{1.1}] to yield the corresponding R(C^{cbz}PNP)CoCl (2ⁱPr-Co^{II}Cl: R = ⁱPr, 88%; 2^tBu-Co^{II}Cl: R = ^tBu, 91%) complexes in high yields (cf. Scheme 1). Due to the paramagnetic nature of d⁷ cobalt complexes and the proximity of the phosphine donors to the metal center, no resonances were detected by ³¹P NMR spectroscopy for the R(C^{cbz}PNP)-

Scheme 1. Synthesis of Chloride Complexes 2ⁱPr-CoCl and 2^tBu-CoCl through in Situ Lithiation of the Protio-ligands and Subsequent Addition of the Co^{II} Precursor



CoCl complexes. Nevertheless, paramagnetic ¹H and ¹³C NMR analysis has proven useful for the characterization of such open shell complexes.^{17a,b} For 2ⁱPr-Co^{II}Cl and 2^tBu-Co^{II}Cl, the paramagnetic ¹H NMR spectra revealed all expected proton resonances except for the methine protons of the ⁱPr groups in 2ⁱPr-Co^{II}Cl, which can be attributed to the proximity to the paramagnetic cobalt center. On the basis of their relative intensities, chemical shifts, and line broadening, all resonances were assigned to their respective atom positions.

The paramagnetic susceptibilities of 2ⁱPr-Co^{II}Cl and 2^tBu-Co^{II}Cl in solution were determined by the Evans method¹⁸ (2ⁱPr-Co^{II}Cl: $\mu_{\text{eff}} = 4.50 \mu_{\text{B}}$; 2^tBu-Co^{II}Cl: $\mu_{\text{eff}} = 4.25 \mu_{\text{B}}$) and were found to agree well with the expected data for d⁷ high-spin complexes. The deviation from the spin-only value (spin-only d⁷: $\mu_{\text{so}} = 3.87 \mu_{\text{B}}$) is consistent with the results previously reported for Co^{II} high-spin complexes and is attributed to a contribution of the orbital angular momentum to the magnetic moment.^{5d,17a,19}

For both complexes, 2ⁱPr-Co^{II}Cl and 2^tBu-Co^{II}Cl, the solid-state structures were determined by X-ray diffraction (cf. Figure 1). The molecular structures confirmed the anticipated

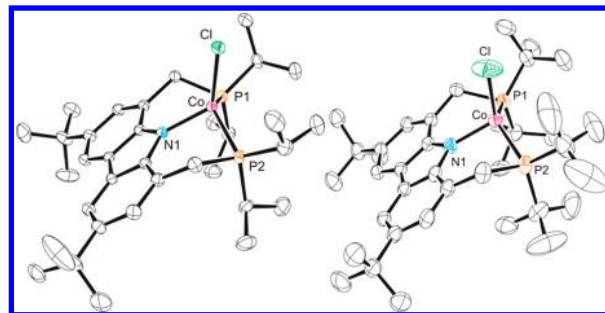


Figure 1. Molecular structures of 2ⁱPr-Co^{II}Cl (left) and 2^tBu-Co^{II}Cl (right). For each structure, only one of the two independent molecules are shown. Hydrogen atoms have been omitted for clarity; displacement ellipsoids are set at 50% probability. Selected bond lengths [Å] and angles [°] (values in square brackets refer to the second independent molecule) 2ⁱPr-Co^{II}Cl: Co–N1 1.9278(18) [1.9315(18)]; Co–P1 2.3354(7) [2.3355(7)]; Co–P2 2.3232(7) [2.3300(7)]; Co–Cl 2.2377(6) [2.2365(7)]; N1–Co–Cl 122.63(6) [124.24(6)]; N1–Co–P1 94.81(6) [96.38(6)]; N1–Co–P2 94.91(8) [94.79(6)]; P1–Co–P2 128.42(3) [129.24(3)]; P1–Co–Cl 108.86(3) [105.65(3)]; P2–Co–Cl 107.71(3) [108.12(3)]. 2^tBu-Co^{II}Cl: Co–N1 1.924(2) [1.919(3)]; Co–P1 2.4075(8) [2.3812(10)]; Co–P2 2.3876(9) [2.3764(10)]; Co–Cl 2.2505(9) [2.2104(11)]; N1–Co–Cl 117.05(8) [110.93(9)]; N1–Co–P1 91.84(7) [98.11(8)]; N1–Co–P2 97.66(7) [97.24(8)]; P1–Co–P2 131.97(3) [135.68(4)]; P1–Co–Cl 106.42(3) [106.99(4)]; P2–Co–Cl 110.46(3) [105.73(5)].

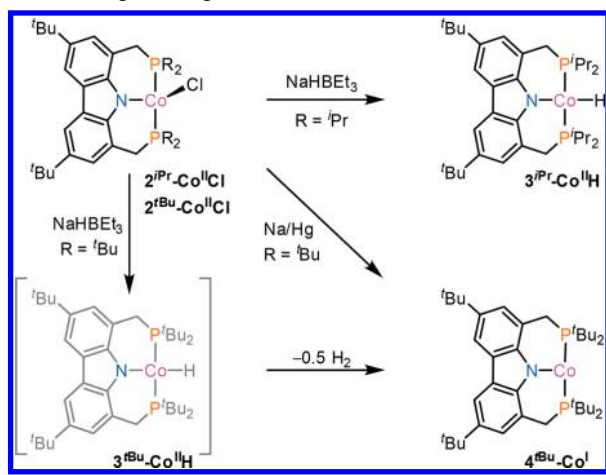
four-coordinated cobalt centers and showed a distorted tetrahedral coordination geometry around the cobalt atom. All metric parameters were found to be as expected and do not differ significantly between the two derivatives. However, there is a notable disparity between the N1–Co–Cl angles. In the case of 2^tBu-Co^{II}Cl, the chlorido ligand appears to be pushed toward the carbazole nitrogen, resulting in a decrease of the N1–Co–Cl angle from 122.6° [124.2°] to 117.1° [110.9°] with respect to 2ⁱPr-Co^{II}Cl, which can be traced back to the increased steric demand of the ^tBu groups compared to the ⁱPr substituents.

Synthesis and Characterization of a Cobalt(II) Hydride and a T-Shaped Cobalt(I) Complex. Chloride

complexes, such as $2^{iPr}\text{-Co}^{\text{II}}\text{Cl}$ and $2^{tBu}\text{-Co}^{\text{II}}\text{Cl}$, are generally convenient starting compounds for the synthesis of alkyl complexes, which in turn can then be reacted with dihydrogen to form the corresponding metal hydrides. Alternatively, metal hydrides may be directly accessed by treating the chloride complexes with hydride transfer reagents such as NaBH_4 , LiAlH_4 , or MHBET_3 ($M = \text{Na}, \text{K}$).^{10c,11}

Treatment of $R(\text{CbzPNP})\text{CoCl}$ complexes $2^{iPr}\text{-Co}^{\text{II}}\text{Cl}$ and $2^{tBu}\text{-Co}^{\text{II}}\text{Cl}$ with NaHBET_3 selectively gave one product species in each case, initially presumed to be the $R(\text{CbzPNP})\text{CoH}$ hydride complexes $3^{iPr}\text{-Co}^{\text{II}}\text{H}$ and $3^{tBu}\text{-Co}^{\text{II}}\text{H}$ (cf. Scheme 2).

Scheme 2. Reactivity of the Chloride Complexes $2^R\text{-Co}^{\text{II}}\text{Cl}$ with NaHBET_3 as well as the Selective Reduction of $2^{tBu}\text{-Co}^{\text{II}}\text{Cl}$ Using Na/Hg



For the latter, a $\nu(\text{Co}-\text{H})$ vibrational band was observed in the IR spectrum, while absent in the $t\text{Bu}$ -substituted derivative. Due to the proximity of the hydride to the paramagnetic cobalt center, the validation of a hydride ligand by its direct detection using NMR spectroscopy was not possible in these cases.

However, determination of the paramagnetic susceptibility in solution by the Evans method¹⁸ gave a magnetic moment of $\mu_{\text{eff}} = 3.13 \mu_{\text{B}}$ for the presumed $t\text{Bu}(\text{CbzPNP})\text{CoH}$ hydride complex $3^{tBu}\text{-Co}^{\text{II}}\text{H}$, which deviated significantly from the expected value for a low-spin d^7 species. On the other hand, a value of $\mu_{\text{eff}} = 2.36 \mu_{\text{B}}$ was determined for $iPr(\text{CbzPNP})\text{Co}$ hydride $3^{iPr}\text{-Co}^{\text{II}}\text{H}$, containing the iPr -substituted PNP pincer, as expected for the formulation of the reaction product. Given the *spin-only* value of low-spin d^7 complexes ($d^7\text{-}l_s: \mu_{\text{so}} = 1.73 \mu_{\text{B}}$), the observed value of $2.36 \mu_{\text{B}}$ is again thought to be due to a contribution of the orbital moment.²⁰

In contrast, the paramagnetic susceptibility of $\mu_{\text{eff}} = 3.13 \mu_{\text{B}}$ for $3^{tBu}\text{-Co}^{\text{II}}\text{H}$ did not match that of a Co^{II} complex but was consistent with that of a *high-spin* Co^{I} complex. In view of the above-mentioned tendency of Co^{II} hydride complexes to undergo reduction,^{11,21} it appeared as though the transformation of $R(\text{CbzPNP})\text{CoCl}$ complexes $2^{iPr}\text{-Co}^{\text{II}}\text{Cl}$ and $2^{tBu}\text{-Co}^{\text{II}}\text{Cl}$ with NaHBET_3 only led to the hydride complex in the case of $3^{iPr}\text{-Co}^{\text{II}}\text{H}$.

To further support this notion, the direct reduction of the Co^{II} complexes $2^R\text{-Co}^{\text{II}}\text{Cl}$ to the corresponding Co^{I} complexes was explored by reacting both chlorido complexes with a variety of reducing agents (Na/Hg , KC_8 , $\text{Mg}(\text{anthracene})\text{-}(\text{thf})_3$). Whereas this only led to an unselective reactivity in the case of $2^{iPr}\text{-Co}^{\text{II}}\text{Cl}$, treating complex $2^{tBu}\text{-Co}^{\text{II}}\text{Cl}$ with Na/Hg selectively yielded the cobalt(I) species $4^{tBu}\text{-Co}^{\text{I}}$ (87%), which

gave rise to identical NMR spectroscopic data as the product isolated from the reaction of 2^{tBu}-CoCl with NaHBET_3 . This indicates that the initial target compound $t\text{Bu}(\text{CbzPNP})\text{CoH}$ ($3^{tBu}\text{-Co}^{\text{II}}\text{H}$) is unstable and readily converted to Co^{I} complex $4^{tBu}\text{-Co}^{\text{I}}$ (cf. Scheme 2).¹¹

To further assess the structural characteristics of complexes $4^{tBu}\text{-Co}^{\text{I}}$ and $3^{iPr}\text{-Co}^{\text{II}}\text{H}$, single crystal X-ray structure analyses of both products were carried out (Figure 2). The cobalt(I)

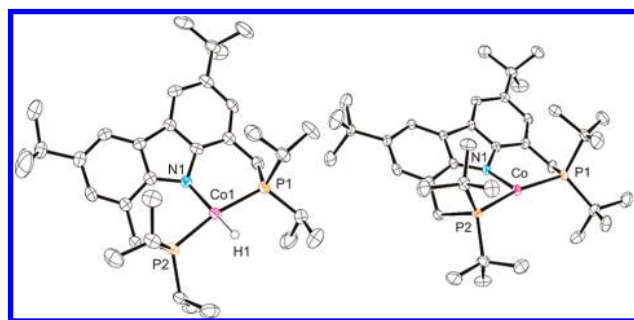


Figure 2. Molecular structures of $3^{iPr}\text{-Co}^{\text{II}}\text{H}$ (left) and $4^{tBu}\text{-Co}^{\text{I}}$ (right). For $3^{iPr}\text{-Co}^{\text{II}}\text{H}$, only one of the two independent molecules is shown. Hydrogen atoms have been omitted for clarity; ellipsoids set at 50% probability. Selected bond lengths [Å] and angles [°] $3^{iPr}\text{-Co}^{\text{II}}\text{H}$: $\text{Co}-\text{N}1$ 1.9454(19); $\text{Co}-\text{P}1$ 2.1710(8); $\text{Co}-\text{P}2$ 2.1768(8); $\text{Co}1-\text{H}1$ 1.45(3); $\text{P}1-\text{Co}1-\text{H}1$ 87.1(10); $\text{P}2-\text{Co}1-\text{H}1$ 81.3(10); $\text{N}1-\text{Co}-\text{P}1$ 95.91(6); $\text{N}1-\text{Co}-\text{P}2$ 96.22(6); $\text{P}1-\text{Co}-\text{P}2$ 167.75(3). $4^{tBu}\text{-Co}^{\text{I}}$: $\text{Co}-\text{N}1$ 1.9872(19); $\text{Co}-\text{P}1$ 2.2351(7); $\text{Co}-\text{P}2$ 2.2273(6); $\text{N}1-\text{Co}-\text{P}1$ 97.80(6); $\text{N}1-\text{Co}-\text{P}2$ 97.77(6); $\text{P}1-\text{Co}-\text{P}2$ 164.43(3).

complex was found to possess the expected T-shaped Co^{I} coordination geometry conferred by the tridentate $t\text{Bu}(\text{CbzPNP})$ ligand ($\text{CoNP}2$ planar within 0.002 Å, Figure 2, right). The molecular structure revealed an elongation of the $\text{N}1-\text{Co}$ bond [1.924(2) to 1.9872(19)] and a contraction of the $\text{P}1/\text{P}2-\text{Co}$ bonds [$\text{P}1-\text{Co}$: 2.4075(8) to 2.2351(7); $\text{P}2-\text{Co}$: 2.3876(9) to 2.2273(6)] compared to the chloride complex $2^{tBu}\text{-Co}^{\text{II}}\text{Cl}$. This is consistent with the change of oxidation state of the metal atom from Co^{II} to Co^{I} and consistent with previously observed metric parameters for such species.^{10c,13a,b}

Due to the change in coordination geometry from distorted tetrahedral to T-shaped, the $\text{P}1-\text{Co}-\text{P}2$ bond angle is significantly increased compared to $2^{tBu}\text{-Co}^{\text{II}}\text{Cl}$. Compared with the only previously described T-shaped Co^{I} complex by Caulton and co-workers,^{2a,13a} the bond lengths of the donor atoms to the cobalt center coincide well with reported structural parameters, whereas the bond angle $\text{P}1-\text{Co}-\text{P}2$ [164.43(3)] is decreased by approximately 6° . The latter may be attributed to the greater rigidity of the PNP pincer employed in this study compared to the more flexible $\text{N}(\text{CH}_2\text{SiMe}_2\text{P}(t\text{Bu})_2)_2$ ligand utilized by Caulton and co-workers.^{13a}

The crystal and molecular structure of $3^{iPr}\text{-Co}^{\text{II}}\text{H}$ (Figure 2, left) is similar to that of the corresponding nickel complex $3^{iPr}\text{-Ni}^{\text{II}}\text{H}$.²² In contrast to $3^{iPr}\text{-Ni}^{\text{II}}\text{H}$, the hydride ligands of both crystallographically independent molecules were located and refined (for details, see the Supporting Information). The cobalt, nitrogen, and both phosphorus atoms also adopt a T-shape arrangement (root-mean-square (RMS) deviation from the plane 0.012 and 0.015 Å), with the hydride ligands displaced from the plane by 0.31(2) and 0.34(2) Å, respectively.

Although the molecular structures established by X-ray diffraction allowed one to rule out a hydride ligand in $4^{\text{tBu}}\text{-Co}^{\text{I}}$ and the refinement of the hydride ligand for $3^{\text{iPr}}\text{-Co}^{\text{IIH}}$, the detection of hydride ligands is sometimes hampered due to the proximity to the metal atom. Therefore, we attempted to unequivocally distinguish between a Co^{I} and a Co^{IIH} complex by an additional spectroscopic technique.

Characterization of Low-Spin Co^{II} Hydride and High-Spin Co^{I} Complexes by Density Functional Theory Supported Paramagnetic NMR Analysis. We have previously employed the density functional theory (DFT) assisted analysis of paramagnetic NMR spectra as a powerful tool for the identification and full characterization of 3d metal complexes.^{15,17a,b} With the Fermi contact shift being the predominant contribution to the paramagnetic shift in ^{13}C NMR spectra of 3d metal complexes, the experimental chemical shifts can be estimated simply by the sum of diamagnetic shift and Fermi contact shift. The latter, in turn, is readily accessible by extracting the unpaired spin density ρ_{af} at a certain NMR active nucleus from quantum chemical calculations, thereby facilitating a reliable prediction of the expected chemical shift of the respective nucleus (for details, see the Supporting Information).

Given the fundamentally different electronic structures in cobalt(II) hydride $3^{\text{R}}\text{-Co}^{\text{IIH}}$ and cobalt(I) species $4^{\text{R}}\text{-Co}^{\text{I}}$, we envisioned that this approach should in principle allow for an unambiguous discrimination between the postulated complexes $3^{\text{iPr}}\text{-Co}^{\text{IIH}}$ as well as $4^{\text{tBu}}\text{-Co}^{\text{I}}$ and the hypothetical alternatives $4^{\text{iPr}}\text{-Co}^{\text{I}}$ and $3^{\text{tBu}}\text{-Co}^{\text{IIH}}$, respectively. Therefore, we calculated the unpaired spin densities ρ_{af} for the four possible species (*low-spin* cobalt(II) hydride and *high-spin* cobalt(I) complex, each for $\text{R} = \text{iPr}, \text{tBu}$) at the DFT level of theory and exploited these for the prediction of chemical shifts.

A schematic representation of the computed ^{13}C NMR spectra is depicted in Figure 3 for the $^{\text{tBu}}$ substituted

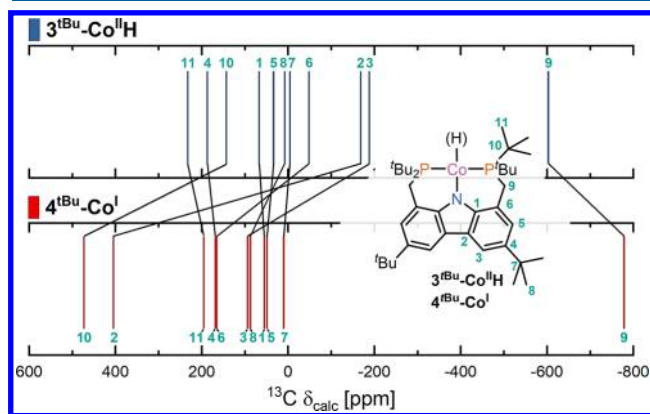


Figure 3. Schematic representation of calculated ^{13}C NMR spectra for a putative $3^{\text{tBu}}\text{-Co}^{\text{IIH}}$ (blue) and $4^{\text{tBu}}\text{-Co}^{\text{I}}$ (red). Signals corresponding to the same nucleus are connected by a straight line.

complexes $3^{\text{tBu}}\text{-Co}^{\text{IIH}}$ and $4^{\text{tBu}}\text{-Co}^{\text{I}}$. As expected, the comparison of both computationally modeled spectra confirmed the expected significant differences in the chemical shifts, giving rise to distinct NMR signal patterns, permitting a clear distinction of the possible complexes on the basis of ^{13}C NMR spectra.

The assignment of the experimentally observed ^{13}C NMR signals of the postulated complexes $3^{\text{tBu}}\text{-Co}^{\text{IIH}}$ and $4^{\text{tBu}}\text{-Co}^{\text{I}}$ was then achieved on the basis of the chemical shifts

(supported by DFT calculations) along with integral values and partially resolved $J(^{31}\text{P}\text{-}^{13}\text{C})$ coupling as well as line width. The correlation between experimentally observed and calculated values was given with sufficient accuracy only for $3^{\text{iPr}}\text{-Co}^{\text{IIH}}$ and $4^{\text{tBu}}\text{-Co}^{\text{I}}$, supporting the above-mentioned structural proposals. This is demonstrated in Figure 4 for the ^{13}C NMR spectrum of $4^{\text{tBu}}\text{-Co}^{\text{I}}$, which gives an excellent correlation with the computed data (red) while being incongruent with the modeled data of the hypothetical $3^{\text{tBu}}\text{-Co}^{\text{IIH}}$ (displayed in blue). A corresponding correlation for $3^{\text{iPr}}\text{-Co}^{\text{IIH}}$ and a hypothetical $4^{\text{iPr}}\text{-Co}^{\text{I}}$ is given in the Supporting Information, confirming the former as the species observed in solution (for details of the NMR study and the DFT modeling, see the Supporting Information).

Since the structures for $3^{\text{R}}\text{-Co}^{\text{IIH}}$ and $4^{\text{R}}\text{-Co}^{\text{I}}$ ($\text{R} = \text{iPr}, \text{tBu}$) were optimized for the NMR analysis, a comparison of the free energies for the $\text{Co}\text{-H}$ and the Co^{I} species has been possible. As expected, the free energy of $3^{\text{iPr}}\text{-Co}^{\text{IIH}}$ was determined to be $\Delta G = -8.2$ kcal/mol below that of $4^{\text{iPr}}\text{-Co}^{\text{I}}$. On the other hand, the $^{\text{tBu}}$ substituted derivative, $3^{\text{tBu}}\text{-Co}^{\text{IIH}}$, has almost equal stability as $4^{\text{tBu}}\text{-Co}^{\text{I}}$ ($\Delta G(3^{\text{tBu}}\text{-Co}^{\text{IIH}}) = -1.9$ kcal/mol). Therefore, it can be assumed that the elimination of H_2 drives the formation of $4^{\text{tBu}}\text{-Co}^{\text{I}}$ from $3^{\text{tBu}}\text{-Co}^{\text{IIH}}$.

Reactions of the Cobalt(I) Complex $4^{\text{tBu}}\text{-Co}^{\text{I}}$. With the assignment of $^{\text{tBu}}(\text{CbzPNP})\text{Co}^{\text{I}}$ ($4^{\text{tBu}}\text{-Co}^{\text{I}}$) and $^{\text{iPr}}(\text{CbzPNP})\text{-Co}^{\text{IIH}}$ ($3^{\text{iPr}}\text{-Co}^{\text{IIH}}$) in hand, we aimed at establishing their reactivity.

Complex $4^{\text{tBu}}\text{-Co}^{\text{I}}$ reacted with carbon monoxide (5 bar) to generate the diamagnetic d^8 *low-spin* carbonyl complex $5^{\text{tBu}}\text{-Co}^{\text{I}}\text{CO}$ in good yields (71%, Scheme 3). The ^{13}C NMR spectroscopic data supports the formation of this species which is characterized by a low field shifted triplet resonance ($\delta(^{13}\text{C}\{^1\text{H}\})$ [ppm] = 207.5 (t, $J_{\text{CP}} = 42$ Hz)) assigned to the CO carbon atom. Further details of the molecular structure were established by X-ray diffraction, which revealed a weakly distorted square planar complex (see the Supporting Information).

In contrast, the reaction of hydride complex $3^{\text{iPr}}\text{-Co}^{\text{IIH}}$ with carbon monoxide did not result in a selective transformation to an identifiable reaction product. Previous reports have shown that Co^{I} complexes coordinate or enable the oxidative addition of dihydrogen.^{13a,23a,b} To explore this reactivity, $4^{\text{tBu}}\text{-Co}^{\text{I}}$ was exposed to a hydrogen atmosphere (10 bar). Under these conditions, $4^{\text{tBu}}\text{-Co}^{\text{I}}$ was found to be in equilibrium with a diamagnetic complex, which was tentatively assigned as the dihydrido complex $6^{\text{tBu}}\text{-Co}^{\text{III}}(\text{H})_2$ based on its ^1H NMR spectrum (Scheme 3), which displayed a distinct triplet resonance ($\delta(^1\text{H})$ [ppm] = -36.98 (t, $J_{\text{HP}} = 61.1$ Hz)) that was assigned to the two hydride ligands of $6^{\text{tBu}}\text{-Co}^{\text{III}}(\text{H})_2$.

Due to the different line broadening of paramagnetic complex $4^{\text{tBu}}\text{-Co}^{\text{I}}$ compared to the diamagnetic complex $6^{\text{tBu}}\text{-Co}^{\text{III}}(\text{H})_2$, the ratio of the two compounds at room temperature could only be estimated ($4^{\text{tBu}}\text{-Co}^{\text{I}}/6^{\text{tBu}}\text{-Co}^{\text{III}}(\text{H})_2 \sim 1:4$).

Whereas the oxidative addition of dihydrogen to $4^{\text{tBu}}\text{-Co}^{\text{I}}$ to yield $6^{\text{tBu}}\text{-Co}^{\text{III}}(\text{H})_2$ is a two-electron process as far as the formal oxidation state of the metal atom is concerned, $4^{\text{tBu}}\text{-Co}^{\text{I}}$ was also found to undergo 1-electron oxidation with substrates favoring radical type transformations. The complex was first reacted with $^{\text{tBu}}\text{Cl}$, giving the deep purple chloride complex $2^{\text{tBu}}\text{-CoCl}$, which was identified by its paramagnetic ^1H and ^{13}C NMR spectra (the $^{\text{tBu}}$ group of $^{\text{tBu}}\text{Cl}$ was not detected by ^1H NMR spectroscopy; thus, a reaction of the $^{\text{tBu}}$ radical with

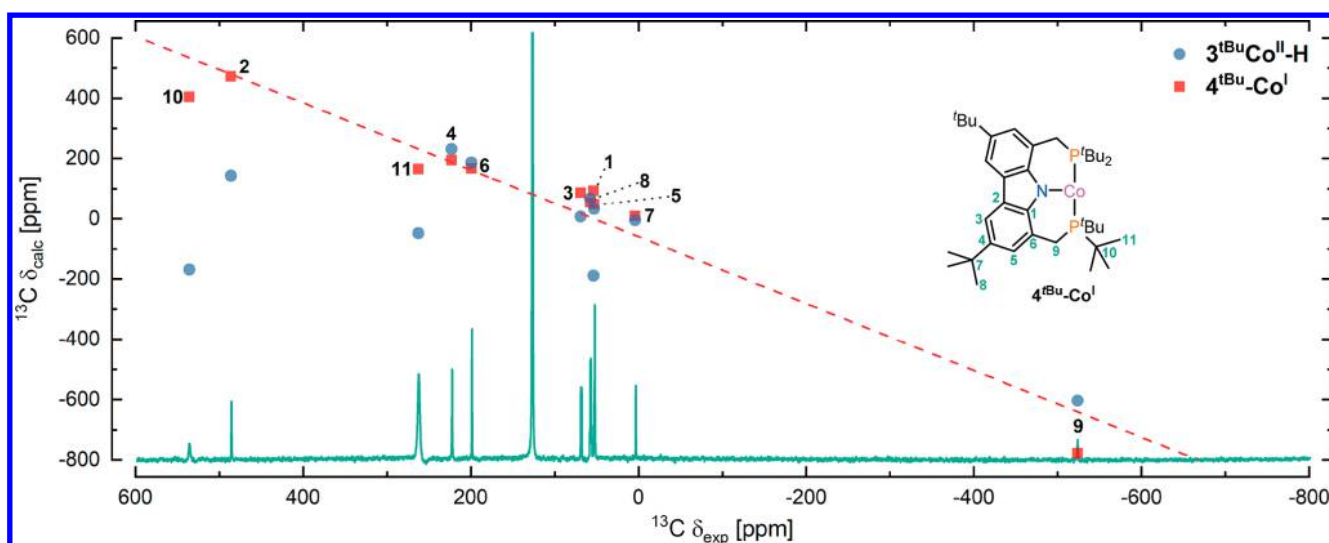
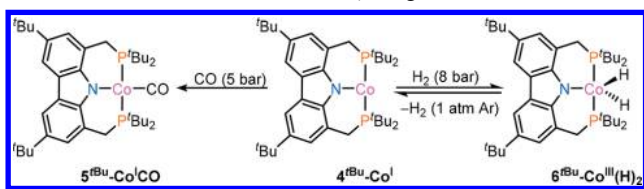


Figure 4. Correlation of experimentally [295 K, 150.92 MHz, C_6D_6] and computationally [B3LYP/6-311(d,p)+TZVP (only for cobalt)] obtained ^{13}C NMR chemical shifts (blue: hypothetical $3^{tBu}\text{-Co}^{II}\text{-H}$ and red: 4^{tBu}-Co^I) for the identification and characterization of cobalt(I) complex 4^{tBu}-Co^I . The dashed line shows the best linear fit for the identified product: slope $m = 1.12$, offset $b = -59.5$, and coefficient of determination $R^2 = 0.94$.

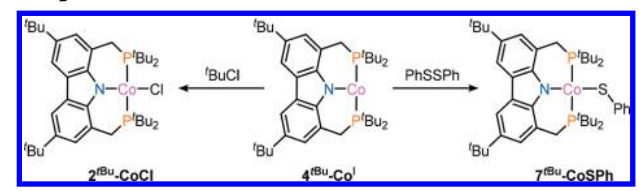
Scheme 3. Reactivity of T-Shaped Co^I Complex 4^{tBu}-Co^I with Carbon Monoxide and Dihydrogen



the solvent via H atom abstraction yielding isobutane is presumed).

This characteristic one-electron oxidative behavior was further demonstrated through reduction of phenyl disulfide to yield the corresponding thiolate complex $7^{tBu}\text{-Co}^{II}\text{SPh}$ (Scheme 4).²⁴

Scheme 4. One-Electron Reactivity of T-Shaped Co^I Complex 4^{tBu}-Co^I



H_2/D_2 and Hydride Exchange at Cobalt(I/III). Since the product of H_2 addition to 4^{tBu}-Co^I could not be isolated and therefore only be characterized by NMR spectroscopy, we further investigated the formation of $6^{tBu}\text{-Co}^{III}(\text{H})_2$, as its formulation as a diamagnetic nonclassical dihydrogen cobalt(I) complex could not be ruled out.^{9d,23b,25} In view of its exchange with its precursor 4^{tBu}-Co^I in solution, ^1H NMR relaxation studies were unsuitable to make that distinction.

For an unambiguous discrimination between a dihydride or a dihydrogen complex, a solution of compound 4^{tBu}-Co^I was placed under an atmosphere of deuterium hydride gas (4 bar at -120°C).²⁶ In case of an oxidative addition step, potentially rapid H–D exchange would be expected, leading to the formation of two product species in the ^1H NMR spectrum,

namely, $6^{tBu}\text{-Co}^{III}(\text{H})_2$ and $6^{tBu}\text{-Co}^{III}\text{HD}$. Indeed, two overlapping resonances at -36.9 and -37.0 ppm were detected almost instantaneously in the $^1\text{H}\{^{31}\text{P}\}$ NMR spectrum after exposure to a 1:1 mixture of H_2 and D_2 at room temperature. Cooling the reaction mixture to -40°C in toluene- d_8 did not result in a significant line narrowing of the hydride signals. However, the resonances for dissolved HD and H_2 gas ($\delta(^1\text{H})$ [ppm] = 4.50 (t, $J_{\text{HD}} = 43$ Hz) and 4.54 (s), respectively) enabled the approximated estimate of the molar ratio of the two dissolved gases. A relative intensity of 1:1 between H_2 and HD was observed in the ^1H NMR spectrum, which represents the statistical distribution of the gases ($\text{H}_2/\text{HD}/\text{D}_2$ of 1:2:1). This equilibrium state is only accessible through isotope scrambling if the dihydrogen isotopomers underwent bond scission to form inter alia $6^{tBu}\text{-Co}^{II}\text{HD}$. This supports the notion of an oxidative addition of H_2 at the cobalt center of 4^{tBu}-Co^I rather than dihydrogen coordination.

In order to obtain insight into the extremely rapid $\text{H}_2/\text{HD}/\text{D}_2$ scrambling, we employed DFT modeling to simulate the essential steps of the HD exchange reaction. In doing so, we were aware of the difficulties previously encountered in DFT modeling studies of reactions involving open shell cobalt and the methodological validation which this required. Notably, Neese and co-workers have encountered cases of extreme variations in the modeling of free energies dependent upon the chosen functionals and basis sets.²⁷ As detailed in the Supporting Information, in the case at hand, the M06L²⁸ functional in combination with the 6-311G(d,p)²⁹ and def2-tzvp (Co)³⁰ basis sets best represented the properties determined experimentally. Nevertheless, while this modeling tool is adequate to arrive at the qualitative distinction of mechanistic alternatives, the computed free energies should be treated with some care.

In principle, we envisioned two different reaction sequences for the HD exchange, with and without the participation of the ligand's amide moiety (Figure 5). Both sequences commence with the oxidative addition of H_2 to the cobalt(I) center of 4^{tBu}-Co^I to form $6^{tBu}\text{-Co}^{III}(\text{H})_2$ ($\Delta G = 4.0$ kcal/mol). As apparent in Figure 5, this transformation is computed to be marginally endergonic; however, experimentally, an equi-

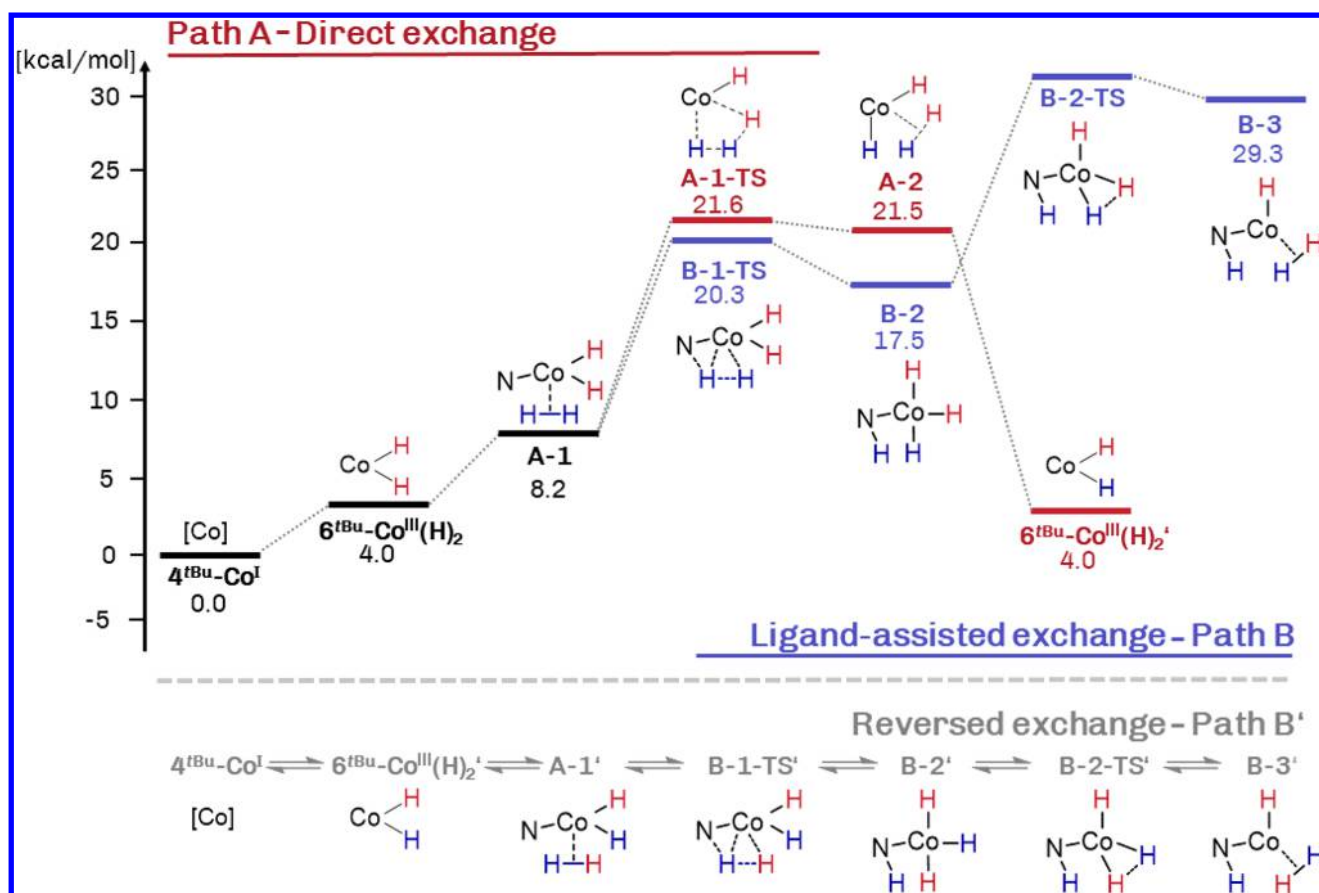


Figure 5. Calculated free energies [kcal mol⁻¹] for reaction Paths A and B with key intermediates and transition states of the conceived HD exchange reaction at 298 K and 8 atm (MO6L/6-311G(d,p), def2TZVP(Co)//def2TZVP/PCM(benzene)). A structure 6^tBu-H₂, without H–H bond constraints, resulted in H₂ bond scission, wherefore no meaningful comparison between the free energies of 6^tBu-Co^IH₂ and 6^tBu-Co^{III}(H)₂ could be made. The extrusion of dihydrogen in B-3 is disfavored (B-4 = 38.4 kcal/mol; cf. Supporting Information).

rium between 4^tBu-Co^I and 6^tBu-Co^{III}(H)₂ of approximately 1:4 is observed. We attribute this on the one hand to the limited computational accuracy, which is achievable on the basis of DFT. On the other hand, it represents a concentration effect on the equilibrium according to Le Chatelier's principle as hydrogen gas is present in excess (8 bar). This is also consistent with the observed instability of 6^tBu-Co^{III}(H)₂ once the hydrogen pressure is released.

Following the reaction path, an additional H₂ molecule coordinates to the cobalt atom forming intermediate A-1 ($\Delta G = 8.2$ kcal/mol; $d(\text{H}-\text{H}) = 0.82$ Å). Path A then proceeds into transition state A-1-TS ($\Delta G^\ddagger = 21.6$ kcal/mol; $d(\text{H}-\text{H}) = 0.99$ Å) through a σ -bond metathesis between the coordinated dihydrogen and one hydride ligand. This results in the intermediate A-2 ($\Delta G = 21.5$ kcal/mol) with a dihydrogen ($d(\text{H}-\text{H}) = 0.89$ Å) *trans*-coordinated to the amide donor. From A-2, the reaction sequence proceeds with the extrusion of the coordinated H₂ to form the “mixed” dihydride 6^tBu-Co^{III}(H)₂'.

Considering the participation of the ligand backbone, a second pathway with a protonated amide moiety is conceivable (Path B, cf. Figure 5).^{4a,8c,31} After the coordination of H₂ to 6^tBu-Co^{III}(H)₂, forming A-1 ($\Delta G = 8.2$ kcal/mol), the H–H bond is cleaved in an endergonic reaction through transition state B-1-TS ($\Delta G^\ddagger(\text{B-1-TS}) = 20.3$ kcal/mol) forming an additional hydride and an amine in the PNP pincer. From B-2 ($\Delta G = 17.5$ kcal/mol), a new H–H bond is created between

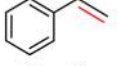
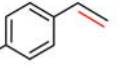
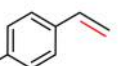
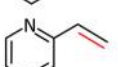
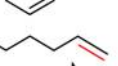
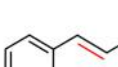
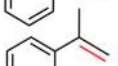
two hydrides generating intermediate B-3 ($\Delta G = 29.3$ kcal/mol) with a coordinated dihydrogen molecule ($d(\text{H}-\text{H}) = 0.88$ Å). The transition state for this bond formation step, B-2-TS, could not be located, presumably because the structural and electronic change between B-2-TS and B-3 is minimal (as it was determined for Path A: A-1-TS and A-2). The extrusion of H₂ from B-3 seems to be the rational subsequent reaction step. However, this extrusion is highly endergonic, and the corresponding intermediate is disfavored by 9.1 kcal/mol compared to B-3 (B-4 = 38.4 kcal/mol; cf. Supporting Information). Therefore, we envisioned a rotation of the coordinated dihydrogen in B-3 to form B-3'. In order to estimate the barrier of this twist, we performed a scan of the N–Co–H–H dihedral angle, simulating a rotation of the H₂ of approximately 180°. This calculation revealed an estimated activation barrier below 2.5 kcal/mol (Figure S2). From B-3', the reaction sequence is reversed to give the mixed dihydride 6^tBu-Co^{III}(H)₂' (Path B', Figure 5, bottom).

Comparison of the computed reaction sequences, A and B, establishes only Path A as feasible at the given reaction conditions. Especially, in view of the fast attainment of the equilibrium state (<1 min at room temperature) in the HD scrambling experiment, the activation barrier of Path B ($\Delta G^\ddagger(\text{Path B}) > 29.3$ kcal/mol) cannot be overcome at the given reaction conditions and renders Path A ($\Delta G^\ddagger(\text{Path A}) = 21.6$ kcal/mol) without the participation of the ligand's amide moiety the only viable reaction sequence.

Putting the Hydrides to Work: Co^{III} Dihydride vs Co^{II} Hydride in Alkene Hydrogenation Reactions. Cobalt hydride complexes have been used as hydrogenation catalysts.^{1d,4a,8b,32} Since two cobalt hydride complexes are accessible employing the ^R(CbzPNP) ligand, we intended to compare the potential activity of the Co^{III} dihydride **6**^{iBu}-Co^{III}(H)₂ versus the Co^{II} hydride complex **3**^{iPr}-Co^{II}H in the catalytic hydrogenation of alkenes. Initially, the activity of both hydride complexes was tested with the privileged substrate norbornene. This revealed a significant difference in the hydrogenation activity: Complex **4**^{iBu}-Co^I did not hydrogenate norbornene under dihydrogen pressure (10 bar) at room temperature, and only a slow transformation into norbornane was observed at 60 °C. In contrast, hydride complex **3**^{iPr}-Co^{II}H readily reduced the test substrate norbornene at 2 mol % in under 5 min at room temperature, which prompted us to further investigate the reactivity of **3**^{iPr}-Co^{II}H in hydrogenation reactions (Table 1).

Table 1. Hydrogenation of Various Alkene Derivatives by **3^{iPr}-Co^{II}H^a**

$$\text{R}-\text{CH}=\text{CH}-\text{R}' \xrightarrow[\text{benzene-d}_6]{[\text{Co}], \text{H}_2} \text{R}-\text{CH}_2-\text{CH}_2-\text{R}'$$

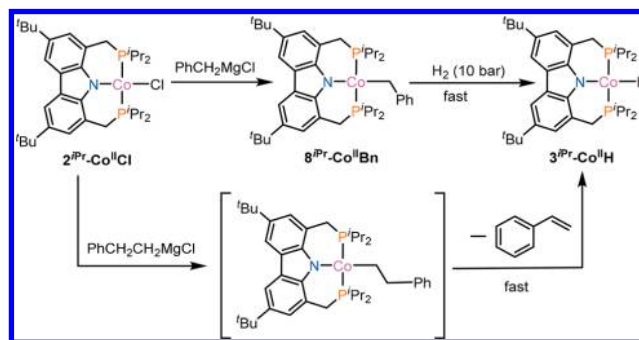
entry	substrate/product	T [°C]	time	^b conversion [%]
1		r.t.	5 min	>99
2		r.t.	5 min	>99
3		r.t.	45 min	95
4		r.t.	44 h	93
5		r.t.	24 h	72
6		r.t.	5 min	>99
7		60	48 h	79
8		60	48 h	59
9		60	48 h	74

^aReaction conditions: 0.5 mL of C₆D₆; *p*(H₂) = 10 bar; 2 mol % of **3**^{iPr}-Co^{II}H; reactions were performed in a Teflon valve pressure tube (New Era, NEPCAV5-M170). ^bConversions were determined by ¹H NMR spectroscopy through integration against ferrocene.

It was found that aryl substituted terminal alkenes were readily hydrogenated (Table 1, Entries 1–4), whereas disubstituted alkenes are only converted over longer periods of time or at elevated temperatures (Table 1, Entries 7–9).

Mechanistically, this can be attributed to a slow insertion step of the alkene into the Co–H bond due to a high stability of hydride complex **3**^{iPr}-Co^{II}H. In principle, this should be observable when the two elementary reactions, alkene insertion and σ -bond metathesis, are carried out independently (Scheme 5). For this purpose, the stoichiometric insertion of 4-

Scheme 5. Stoichiometric Transformations Modeling Elementary Reaction Steps of the Hydrogenation Mechanism of Alkenes



fluorostyrene into the Co–H bond of **3**^{iPr}-Co^{II}H was examined. Utilizing ¹H and ¹⁹F NMR spectroscopy, a conversion to an alkyl complex was not detected; however, an increased line-broadening of the ¹⁹F resonance of 4-fluorostyrene was noticed.

Given these observations, we presumed an equilibrium between insertion of the alkene and a predominant β -H elimination reforming **3**^{iPr}-Co^{II}H. Furthermore, the line-broadening of the ¹⁹F resonance can be attributed to rapid exchange involving weak coordination of the alkene to the cobalt center. To probe this hypothesis, **2**^{iPr}-Co^{II}Cl was treated with a solution of phenethylmagnesium chloride. This directly resulted in the formation of **3**^{iPr}-Co^{II}H, verifying the fast attainment of the equilibrium's steady state via β -H elimination of the alkene insertion product. Despite complete conversion to **3**^{iPr}-Co^{II}H, styrene was only detected in the ¹H NMR spectrum after filtration over silica, supporting the presumed coordination to the paramagnetic cobalt center.

Further evidence of the insertion/ β -H elimination equilibrium was obtained by the reaction of complex **3**^{iPr}-Co^{II}D with neat styrene. This led to a deuterium incorporation into styrene, which was observed by ²H NMR spectroscopy (cf. Supporting Information), proving the reversibility of insertion and deinsertion. The second elementary reaction, the σ -bond metathesis of H₂ with the Co–C bond, was demonstrated through the reaction of benzyl complex ^{iPr}(CbzPNP)CoCH₂Ph, **8**^{iPr}-Co^{II}Bn, with dihydrogen at elevated pressure (10 bar). In this reaction, a rapid cleavage of the Co–C bond to yield hydride complex **3**^{iPr}-Co^{II}H was observed.

From these findings, we presume that a slow insertion of the alkene is the limiting step in the hydrogenation catalyzed by **3**^{iPr}-Co^{II}H. Therefore, the insertion of disubstituted alkenes is less likely to proceed as the steric demand of the alkenes increases, resulting in the longer reaction times for disubstituted alkenes (Table 1, Entries 7–9). Furthermore, it cannot be ruled out that coordination of dihydrogen under catalytic conditions (10 bar H₂) facilitates the insertion of the alkene in the Co–H bond.

CONCLUSION

In this study, we have shown that a minor change in steric demand of the P-substituents in the pincer ligands ^{iPr}(CbzPNP) to ^{iBu}(CbzPNP) results in a remarkable difference of reactivity when coordinated to a cobalt atom. It enabled the selective synthesis of both a cobalt(II) hydride and a three-coordinate cobalt(I) complex; to our knowledge, this is only the second

such example to be fully characterized. As X-ray structure analysis left some ambiguity in distinguishing between the observed $\text{Co}^{\text{II}}\text{-H}$ and Co^{I} complexes, which result from halide for hydride exchange, we have utilized DFT-assisted evaluation of paramagnetic NMR spectra to establish the existence of $3^{\text{iPr}}\text{-Co}^{\text{II}}\text{H}$ and $4^{\text{tBu}}\text{-Co}^{\text{I}}$ unambiguously. Apart from the expected one-electron reactivity with $^{\text{tBu}}\text{Cl}$ and PhSSPh , $4^{\text{tBu}}\text{-Co}^{\text{I}}$ also reacted with dihydrogen under oxidative addition to its metal center to form the dihydride complex $6^{\text{tBu}}\text{-Co}^{\text{III}}(\text{H})_2$. The cleavage of H_2 in the process was demonstrated in the rapid exchange between the isotopomers $\text{H}_2/\text{HD}/\text{D}_2$ upon exposure to a mixture of H_2 and D_2 . Whereas the cobalt(III) dihydrido complex $6^{\text{tBu}}\text{-Co}^{\text{III}}(\text{H})_2$ showed little reactivity in the hydrogenation of alkenes, the cobalt(II) monohydride $3^{\text{iPr}}\text{-Co}^{\text{II}}\text{H}$ was found to readily catalyze the hydrogenation of monosubstituted alkenes.

EXPERIMENTAL SECTION

Computational Methods. All calculations were carried out using density functional theory (DFT) employing the Gaussian 09³³ package. As previously established,^{17a,34} the spin densities for the NMR shift determinations were calculated with the B3LYP functional.^{35a,b} In the optimization and frequency calculation, the atoms C, H, N, and P were represented with the 6-311G(d,p)²⁹ basis set and Co, with the def2-tzvp³⁰ basis set.

The determination of a viable functional was conducted in two separate steps. Initially, complex $4^{\text{tBu}}\text{-Co}^{\text{I}}$ was computed with three different well established functionals, B3LYP,^{35a,b} PBE0,³⁶ and M06L²⁸ as well as two basis sets for nonmetal atoms (6-311G(d,p)²⁹ and def2svp³⁷). Subsequently, the obtained bond lengths of the donor atoms to the metal center were compared with those of the obtained molecular structure of $4^{\text{tBu}}\text{-Co}^{\text{I}}$ (cf. Table S1). Additionally, the first three intermediates of the HD exchange mechanism, $4^{\text{tBu}}\text{-Co}^{\text{I}}$, $6^{\text{tBu}}\text{-III}(\text{H})_2$, and A-1, were computed, and the energies compared (cf. Figure S2). It turned out that the M06L²⁸ functional in combination with the 6-311G(d,p)²⁹ and def2-tzvp (Co)³⁰ basis sets best represented the properties determined experimentally. Therefore, this functional and these basis sets were utilized in geometry optimizations for the HD exchange reaction sequence. Frequency calculations were carried out with def2-tzvp for all atoms. The solvent (benzene) influence was considered by an additional SCRF calculation within the PCM³⁸ model, employing the def2-tzvp³⁰ basis set for all atoms. Energies are reported as Gibbs free energies, including the gas-phase Gibbs contributions at 298 K and 8 atm. Vibrational modes below -100 cm^{-1} were replaced by 100 cm^{-1} as suggested by Cramer and co-workers³⁹ using the GoodVibes⁴⁰ program developed by Funes-Ardoiz and Paton. All DFT-optimized structures are provided in a separate XYZ file, and a detailed description of computational proceedings can be found in the Supporting Information.

Synthetic Procedures. $^{\text{iPr}}(\text{CbzPnP})\text{CoCl}$ ($2^{\text{iPr}}\text{-Co}^{\text{II}}\text{Cl}$). A solution of $^{\text{iPr}}(\text{CbzPnP})\text{H}$ (1^{Pr}) (1.0 g, 1.85 mmol, 1.0 equiv) in toluene (10 mL) was treated with a solution of LiHMDS (341 mg, 2.04 μmol , 1.1 equiv) in toluene (5 mL) and stirred for 15 min. Subsequently, solid $[\text{CoCl}_2(\text{thf})_{1.1}]$ (412 mg, 2.04 μmol , 1.1 equiv) was added in portions. After 4 h, the reaction mixture was filtrated over Celite; the solvent was removed under vacuum, and the residue was washed with *n*-pentane to yield a crystalline, purple product (1.03 g, 1.63 mmol, 88%). $\mu_{\text{eff}} = 4.50\ \mu_{\text{B}}$. $^1\text{H NMR}$ (600.13 MHz, toluene- d_6 , 293 K): δ [ppm] = 333.4 (s, 4H, CH_2), 197.1 (s, 2H, $\text{CH}(\text{CH}_3)_2$), 170.0 (s, 2H, $\text{CH}(\text{CH}_3)_2$), 61.1 (s, 2H, H_{Carb}), 18.1 (s, 2H, H_{Carb}), 9.8 (s, 12H, $\text{CH}(\text{CH}_3)_2$), 5.0 (s, 18H, $\text{C}(\text{CH}_3)_3$), -4.6 (s, 12H, $\text{CH}(\text{CH}_3)_2$). $^{13}\text{C NMR}$ (150.90 MHz, toluene- d_6 , 355 K): δ [ppm] = 842.8 (s, CH_2), 425.7 (s, C_{Carb}), 401.1 (s, C_{Carb}), 153.1 (s, $\text{CH}(\text{CH}_3)_2$), 116.5 (q, $J = 123.0\text{ Hz}$, $\text{C}(\text{CH}_3)_3$), 25.1 (s, $\text{CH}(\text{CH}_3)_2$), -12.5 (d, $J = 136.5\text{ Hz}$, $\text{C}_{\text{Carb-3/5}}$), -53.3 (s, $\text{C}(\text{CH}_3)_3$), -52.3 (d, $J = 140.0\text{ Hz}$, $\text{C}_{\text{Carb-3/5}}$). Anal. Calcd for $\text{C}_{34}\text{H}_{54}\text{CoNP}_2\text{Cl}$: C, 64.50; H, 8.60; N, 2.21. Found: C, 64.71; H, 8.10; N, 2.22.

$^{\text{iPr}}(\text{CbzPnP})\text{CoH}$ ($3^{\text{iPr}}\text{-Co}^{\text{II}}\text{H}$). A solution of $2^{\text{iPr}}\text{-Co}^{\text{II}}\text{Cl}$ (16 mg, 316 μmol , 1.0 equiv) in toluene (5 mL) was treated with a 1 M solution of NaHBET_3 (316 μL , 316 mmol, 1.0 equiv) in toluene. The resulting mixture was stirred for 2 h and filtrated using a syringe filter, and the solvent was removed. After washing the residue with *n*-pentane (0.5 mL), the product was obtained as an orange solid (100 mg, 167 μmol , 53%). $\mu_{\text{eff}} = 2.36\ \mu_{\text{B}}$. $^1\text{H NMR}$ (600.13 MHz, C_6D_6 , 295 K): δ [ppm] = 48.7 (s, 4H, $\text{CH}_2/\text{CH}(\text{CH}_3)_2$), 37.1 (s, 4H, $\text{CH}_2/\text{CH}(\text{CH}_3)_2$), 26.2 (s, 2H, H_{Carb}), 7.6 (bs, 12H, $\text{PCH}(\text{CH}_3)_2$), 2.4 (s, 18H, $\text{C}(\text{CH}_3)_3$), 0.1 (s, 2H, H_{Carb}), -8.2 (bs, 12H, $\text{PCH}(\text{CH}_3)_2$). $^{13}\text{C NMR}$ (150.90 MHz, C_6D_6 , 295 K): δ [ppm] = 196.2 (s, $\text{C}_{\text{Carb-4}}$), 175.3 (s, $\text{C}_{\text{Carb-6}}$), 115.3 (s, $\text{C}_{\text{Carb-2}}$), 88.2 (d, $J = 130.9\text{ Hz}$, $\text{C}_{\text{Carb-3/5}}$), 84.7 (s, $\text{CH}(\text{CH}_3)_2$), 83.0 (s, $\text{CH}(\text{CH}_3)_2$), 53.0 (d, $J = 156.5\text{ Hz}$, $\text{C}_{\text{Carb-3/5}}$), 30.8 (q, $J = 124.8$, 124.1 Hz, $\text{C}(\text{CH}_3)_3$), 15.3 (s, $\text{C}(\text{CH}_3)_3$), -30.4 (s, $\text{CH}(\text{CH}_3)_2$), -98.0 (s, $\text{C}_{\text{Carb-1}}$), -298.4 (s, CH_2). IR: ν_{CoH} (KBr), cm^{-1} 1820. Anal. Calcd for $\text{C}_{34}\text{H}_{55}\text{CoNP}_2$: C, 68.21; H, 9.26; N, 2.34. Found: C, 68.29; H, 9.16; N, 2.19.

$^{\text{tBu}}(\text{CbzPnP})\text{CoCl}$ ($2^{\text{tBu}}\text{-Co}^{\text{II}}\text{Cl}$). A solution of $^{\text{tBu}}(\text{CbzPnP})\text{H}$ (1^{tBu}) (1.0 g, 1.68 mol, 1.0 equiv) in toluene (5 mL) was treated with a solution of LiHMDS (295 mg, 1.76 mmol, 1.05 equiv) in toluene (2 mL) and stirred for 15 min. Subsequently, solid $[\text{CoCl}_2(\text{thf})_{1.1}]$ (185 mg, 1.76 mmol, 1.05 equiv) was added in portions. After 4 h, the reaction mixture was filtrated over Celite; the solvent was removed under vacuum, and the residue was washed with *n*-pentane to yield a crystalline, purple product (1.05 g, 1.52 mmol, 91%). $\mu_{\text{eff}} = 4.25\ \mu_{\text{B}}$. $^1\text{H NMR}$ (600.13 MHz, C_6D_6 , 295 K): δ [ppm] = 138.1 (s, 4H, CH_2), 63.9 (s, 2H, H_{Carb}), 24.4–17.4 (bs, 18H, $\text{PC}(\text{CH}_3)_3$), 16.8 (s, 2H, H_{Carb}), 5.1 (s, 18H, $\text{C}(\text{CH}_3)_3$), 3.4 (bs, 18H, $\text{PC}(\text{CH}_3)_3$). $^{13}\text{C NMR}$ (150.90 MHz, C_6D_6 , 295 K): δ [ppm] = 797.6 (s), 526.6 (s), 464.8 (s), 411.7 (s), 349.0 (s), 285.9 (s), 195.4 (s), 119.5 (q, $J = 124.5\text{ Hz}$), -3.2 (d, $J = 137.0\text{ Hz}$), -56.2 (s), -64.3 (d, $J = 140.5\text{ Hz}$), -75.6 (s).

$^{\text{tBu}}(\text{CbzPnP})\text{Co}$ ($4^{\text{tBu}}\text{-Co}^{\text{I}}$). A solution of $2^{\text{tBu}}\text{-Co}^{\text{II}}\text{Cl}$ (600 mg, 871 μmol , 1.0 equiv) in THF (10 mL) was cooled to $-40\text{ }^\circ\text{C}$ and slowly added to a stirring mixture of Na/Hg (24 mg, 958 μmol , 1.1 equiv. Na in 2.5 g of Hg). The mixture was allowed to warm to room temperature and stirred overnight. After the organic phase was extracted, the solvent was removed under vacuum. The residue was absorbed with *n*-pentane and filtrated over Celite. After the solvent was removed, the product was obtained as a green solid (495 mg, 757 μmol , 87%). $\mu_{\text{eff}} = 3.13\ \mu_{\text{B}}$. $^1\text{H NMR}$ (600.13 MHz, C_6D_6 , 295 K): δ [ppm] = 29.0 (s, 2H, H_{Carb}), 17.3 (s, 4H, CH_2), 13.0 (s, 2H, H_{Carb}), 11.0 (s, 36H, $\text{PC}(\text{CH}_3)_3$), 1.9 (s, 18H, $\text{C}(\text{CH}_3)_3$). $^{13}\text{C NMR}$ (150.90 MHz, C_6D_6 , 295 K): δ [ppm] = 536.9 (s, $\text{PC}(\text{CH}_3)_3$), 487.0 (s, $\text{C}_{\text{Carb-2}}$), 263.5 (s, $\text{PC}(\text{CH}_3)_3$), 224.0 (s, $\text{C}_{\text{Carb-4}}$), 200.3 (s, $\text{C}_{\text{Carb-6}}$), 69.8 (d, $\text{C}_{\text{Carb-3}}$), 58.6 (q, $\text{C}(\text{CH}_3)_3$), 54.4–53.7 (m, $\text{C}_{\text{Carb-5}}$, $\text{C}_{\text{Carb-1}}$), 4.8 (s, $\text{C}(\text{CH}_3)_3$), -521.9 (s, CH_2). Anal. Calcd for $\text{C}_{38}\text{H}_{62}\text{CoNP}_2$: C, 69.81; H, 9.56; N, 2.14. Found: C, 69.53; H, 9.38; N, 2.22.

$^{\text{tBu}}(\text{CbzPnP})\text{Co}(\text{H})_2$ ($6^{\text{tBu}}\text{-Co}^{\text{III}}(\text{H})_2$). In a high-pressure NMR tube, a solution of $4^{\text{tBu}}\text{-Co}^{\text{I}}$ (20 mg, 31 μmol) in benzene- d_6 was exposed to a dihydrogen atmosphere (8 bar) resulting in an instant color conversion from a green to a dark green/brown solution and an equilibrium of dihydride complex $6^{\text{tBu}}\text{-Co}^{\text{III}}(\text{H})_2$ to reagent $4^{\text{tBu}}\text{-Co}^{\text{I}}$ with a ratio of 4:1 at 295 K. Complex $6^{\text{tBu}}\text{-Co}^{\text{III}}(\text{H})_2$ is only stable under hydrogen pressure. $^1\text{H NMR}$ (600.13 MHz, C_6D_6 , 295 K): δ [ppm] = 8.31 (s, 2H, $\text{H}_{\text{Carb-3}}$), 7.43 (s, 2H, $\text{H}_{\text{Carb-5}}$), 3.43 (s, 4H, CH_2), 1.59 (s, 18H, $\text{C}(\text{CH}_3)_3$), 1.13–1.11 (m, 36H, $\text{PC}(\text{CH}_3)_3$), -37.0 (t, 2H, $J_{\text{HP}} = 61.1\text{ Hz}$, $\text{Co}(\text{H})_2$). $^{13}\text{C NMR}$ (150.90 MHz, C_6D_6 , 295 K): δ [ppm] = 147.5 (s, $\text{C}_{\text{Carb-1}}$), 138.3 (s, $\text{C}_{\text{Carb-4}}$), 125.9 (s, $\text{C}_{\text{Carb-2}}$), 122.7 (s, $\text{C}_{\text{Carb-5}}$), 120.9 (s, $\text{C}_{\text{Carb-6}}$), 113.8 (s, $\text{C}_{\text{Carb-3}}$), 33.8 (t, $J = 9.7\text{ Hz}$, $\text{PC}(\text{CH}_3)_3$), 33.5 (s, $\text{C}(\text{CH}_3)_3$), 31.3 (s, $\text{C}(\text{CH}_3)_3$), 28.3 (s, $\text{PC}(\text{CH}_3)_3$), 22.1 (s, CH_2).

$^{\text{tBu}}(\text{CbzPnP})\text{CoCo}$ ($5^{\text{tBu}}\text{-Co}^{\text{I}}\text{Co}$). In a high-pressure NMR tube, a solution of $4^{\text{tBu}}\text{-Co}^{\text{I}}$ (31 mg, 47 μmol) in benzene- d_6 was exposed to a carbon monoxide atmosphere (5 bar). After removal of the solvent, the residue was washed with *n*-pentane. The product was obtained as a light purple solid (23 mg, 34 μmol , 71%). $^1\text{H NMR}$ (600.13 MHz, C_6D_6 , 295 K): δ [ppm] = 8.28 (d, $J = 1.9\text{ Hz}$, 2H, $\text{H}_{\text{Carb-3}}$), 7.31 (d, $J = 1.9\text{ Hz}$, 2H, $\text{H}_{\text{Carb-5}}$), 3.22–3.17 (m, 4H, CH_2), 1.58 (s, 18H, $\text{C}(\text{CH}_3)_3$), 1.39–1.32 (m, 36H, $\text{PC}(\text{CH}_3)_3$). $^{13}\text{C NMR}$ (150.90 MHz,

C_6D_6 , 295 K): δ [ppm] = 207.5 (t, J = 42 Hz, CO), 149.48 (s, C_{Carb-1}), 139.31 (s, C_{Carb-4}), 126.05 (s, C_{Carb-2}), 122.85 (t, J = 3.3 Hz, C_{Carb-5}), 120.35 (s, C_{Carb-6}), 114.83 (s, C_{Carb-3}), 36.64 (t, J = 8.2 Hz, $PC(CH_3)_3$), 34.65 (s, $C(CH_3)_3$), 32.51 (s, $C(CH_3)_3$), 30.25 (s, $PC(CH_3)_3$), 22.79 (t, J = 4.4 Hz, CH_2). ^{31}P NMR (242.94 MHz, C_6D_6 , 295 K): δ (ppm) = 76.2 (s). IR: ν_{CO} (KBr), cm^{-1} 1886. Anal. Calcd for $C_{39}H_{62}CoNOP_2$: C, 68.70; H, 9.17; N, 2.05. Found: C, 68.65; H, 9.47; N, 2.07.

$^{tBu}(CbzPNP)CoSPh$ ($7^{tBu}-Co^I SPh$). To a solution of $4^{tBu}-Co^I$ (10 mg, 16 μ mol, 2.0 equiv) in benzene- d_6 was added solid diphenyl disulfide (1.7 mg, 8 μ mol, 1 equiv). The reaction mixture was stirred for 5 min; all volatiles were removed, and the title product was obtained as purple solid (9.6 mg, 10 μ mol, 68%). μ_{eff} = 4.3 μ_B . 1H NMR (600.13 MHz, C_6D_6 , 295 K): δ [ppm] = 265.4 (s, 2H, CH_2), 149.7 (s, 2H, CH_2), 57.6 (s, 2H, H_{Carb}/H_{Ph}), 24.5 (s, 2H, H_{Carb}/H_{Ph}), 14.7 (s, 2H, H_{Carb}/H_{Ph}), 14.3–13.4 (m, 18H, $PC(CH_3)_3$), 11.1–9.6 (m, 18H, $PC(CH_3)_3$), 3.8 (s, 18H, $C(CH_3)_3$), –41.1 (s, 1H, H_{Ph}), –54.2 (s, 2H, H_{Ph}). ^{13}C NMR (150.90 MHz, C_6D_6 , 295 K): δ [ppm] = 771.4 (s), 726.2 (s), 485.9 (s), 474.1 (s), 436.4 (s), 346.7 (d, J = 158.3 Hz), 267.2 (s), 264.4 (s), 206.4 (s), 123.0 (q, J = 125.1 Hz), 36.3 (d, J = 151.6 Hz), –29.2 (d, J = 143.2 Hz), –31.0 (s), –63.8 (s), –85.6 (d, J = 145.0 Hz). Anal. Calcd for $C_{44}H_{67}CoNSP_2$: C, 69.27; H, 8.85; N, 1.84. Found: C, 68.99; H, 8.94; N, 1.85.

$^{iPr}(CbzPNP)CoBn$ ($8^{iPr}-Co^II Bn$). To a solution of $2^{iPr}-Co^II Cl$ (50 mg, 79 mmol, 1.0 equiv) in toluene (2 mL) was slowly added $Bn_2Mg(thf)_2$ (28 mg, 79 mmol, 1.0 equiv) in toluene (1 mL). The resulting mixture was stirred for 2 h, and then, all volatiles were removed. The residue was suspended in *n*-pentane and filtrated using a syringe filter, and the solvent was removed. The product was obtained as a deep red solid (30 mg, 44 μ mol, 55%). μ_{eff} = 4.0 μ_B . 1H NMR (600.13 MHz, C_6D_6 , 295 K): δ [ppm] = 50.0 (s, 2H, CH_2), 35.2 (s, 2H, CH_2), 14.6 (s, 2H, $H_{Carb-3/5}$), 11.1 (s, 12H, $CH(CH_3)_2$), 5.5 (s, 18H, $C(CH_3)_3$), 3.6 (s, 12H, $CH(CH_3)_2$), 0.9 (s, 2H, $H_{Carb-3/5}$), –84.3 (s, 2H, H_{Ph}), –91.9 (s, 1H, H_{Ph}). ^{13}C NMR (151 MHz, C_6D_6 , 295 K) δ [ppm] = 649.2 (s), 419.5 (s), 365.2 (s), 324.6 (s), 104.1 (q, J = 123.6 Hz), 84.5 (s), 11.7 (d, J = 138.5 Hz), –21.9 (d, J = 136.7 Hz), –41.6 (s), –301.4 (s). Anal. Calcd for $C_{41}H_{61}CoNP_2$: C, 71.49; H, 8.93; N, 2.03. Found: C, 71.19; H, 9.29; N, 2.38.

ASSOCIATED CONTENT

Supporting Information

The Supporting Information is available free of charge on the ACS Publications website at DOI: 10.1021/acs.inorgchem.9b00384.

Experimental details and characterization data of all new compounds, synthetic protocols, spectral data, and X-ray crystallographic information (PDF)

DFT-optimized geometries (XYZ)

Accession Codes

CCDC 1882792–1882796 and 1895478 contain the supplementary crystallographic data for this paper. These data can be obtained free of charge via www.ccdc.cam.ac.uk/data_request/cif, or by emailing data_request@ccdc.cam.ac.uk, or by contacting The Cambridge Crystallographic Data Centre, 12 Union Road, Cambridge CB2 1EZ, UK; fax: +44 1223 336033.

AUTHOR INFORMATION

Corresponding Author

*E-mail: lutz.gade@uni-heidelberg.de.

ORCID

Lutz H. Gade: 0000-0002-7107-8169

Notes

The authors declare no competing financial interest.

ACKNOWLEDGMENTS

The authors thank Heidelberg University for funding this work and acknowledge support by the state of Baden-Württemberg through bwHPC. Further gratitude is owed to M. Enders for fruitful discussions regarding NMR analysis. In addition, we thank D. Laible and H. Ruppert for experimental support.

DEDICATION

This paper is dedicated to Helmut Werner on the occasion of this 85th birthday.

REFERENCES

- (a) Bullock, R. M., Ed. *Catalysis without Precious Metals*; Wiley-VCH Verlag GmbH & Co. KGaA: Weinheim, Germany, 2010.
- (b) Morris, R. H. Asymmetric Hydrogenation, Transfer Hydrogenation and Hydrosilylation of Ketones Catalyzed by Iron Complexes. *Chem. Soc. Rev.* **2009**, *38*, 2282.
- (c) Zell, T.; Milstein, D. Hydrogenation and Dehydrogenation Iron Pincer Catalysts Capable of Metal-Ligand Cooperation by Aromatization/ Dearomatization. *Acc. Chem. Res.* **2015**, *48*, 1979–1994.
- (d) Chirik, P. J. Iron- and Cobalt-Catalyzed Alkene Hydrogenation: Catalysis with Both Redox-Active and Strong Field Ligands. *Acc. Chem. Res.* **2015**, *48*, 1687–1695.
- (e) Su, B.; Cao, Z.-C.; Shi, Z.-J. Exploration of Earth-Abundant Transition Metals (Fe, Co, and Ni) as Catalysts in Unreactive Chemical Bond Activations. *Acc. Chem. Res.* **2015**, *48*, 886–896.
- (f) Filonenko, G. A.; van Putten, R.; Hensen, E. J. M.; Pidko, E. A. Catalytic (de)Hydrogenation Promoted by Non-Precious Metals - Co, Fe and Mn: Recent Advances in an Emerging Field. *Chem. Soc. Rev.* **2018**, *47*, 1459–1483.
- (g) Chirik, P. J.; Wieghardt, K. Radical Ligands Confer Nobility on Base-Metal Catalysts. *Science* **2010**, *327*, 794–795.
- (h) Langlotz, B. K.; Wadepohl, H.; Gade, L. H. Chiral Bis(Pyridylimino)Isoindoles: A Highly Modular Class of Pincer Ligands for Enantioselective Catalysis. *Angew. Chem., Int. Ed.* **2008**, *47*, 4670–4674.
- (i) Inagaki, T.; Phong, L. T.; Furuta, A.; Ito, J.; Nishiyama, H. Iron- and Cobalt-Catalyzed Asymmetric Hydrosilylation of Ketones and Enones with Bis(Oxazolinyphenyl)Amine Ligands. *Chem. - Eur. J.* **2010**, *16*, 3090–3096.
- (j) Monfette, S.; Turner, Z. R.; Semproni, S. P.; Chirik, P. J. Enantiopure C 1-Symmetric Bis(Imino)Pyridine Cobalt Complexes for Asymmetric Alkene Hydrogenation. *J. Am. Chem. Soc.* **2012**, *134*, 4561–4564.
- (k) Gandeepan, P.; Cheng, C.-H. Cobalt Catalysis Involving π Components in Organic Synthesis. *Acc. Chem. Res.* **2015**, *48*, 1194–1206.
- (l) Bigler, R.; Huber, R.; Mezzetti, A. Highly Enantioselective Transfer Hydrogenation of Ketones with Chiral $(NH)_2P_2$ Macrocyclic Iron(II) Complexes. *Angew. Chem., Int. Ed.* **2015**, *54*, 5171–5174.
- (m) Zuo, Z.; Zhang, L.; Leng, X.; Huang, Z. Iron-Catalyzed Asymmetric Hydrosilylation of Ketones. *Chem. Commun.* **2015**, *51*, 5073–5076.
- (n) Vasilenko, V.; Blasius, C. K.; Wadepohl, H.; Gade, L. H. Mechanism-Based Enantiodivergence in Manganese Reduction Catalysis: A Chiral Pincer Complex for the Highly Enantioselective Hydroboration of Ketones. *Angew. Chem., Int. Ed.* **2017**, *56*, 8393–8397.
- (o) Blasius, C. K.; Vasilenko, V.; Gade, L. H. Ultrafast Iron-Catalyzed Reduction of Functionalized Ketones: Highly Enantioselective Synthesis of Halohydrines, Oxaheterocycles, and Aminoalcohols. *Angew. Chem., Int. Ed.* **2018**, *57*, 10231–10235.
- (p) Kallmeier, F.; Kempe, R. Manganese Complexes for (De)-Hydrogenation Catalysis: A Comparison to Cobalt and Iron Catalysts. *Angew. Chem., Int. Ed.* **2018**, *57*, 46–60.
- (2) (a) Ingleson, M. J.; Pink, M.; Caulton, K. G. Reducing Power of Three-Coordinate Cobalt(I). *J. Am. Chem. Soc.* **2006**, *128*, 4248–4249.
- (b) Poli, R. Relationship between One-Electron Transition-Metal Reactivity and Radical Polymerization Processes. *Angew. Chem., Int. Ed.* **2006**, *45*, 5058–5070.
- (c) Dhuri, S. N.; Seo, M. S.; Lee, Y.-M.; Hirao, H.; Wang, Y.; Nam, W.; Shaik, S. Experiment and Theory Reveal the Fundamental Difference between Two-State and Single-State Reactivity Patterns in Nonheme $Fe^{IV}=O$ versus $Ru^{IV}=O$ Oxidants. *Angew. Chem., Int. Ed.* **2008**, *47*, 3356–3359.
- (d) Palmer,

W. N.; Diao, T.; Pappas, I.; Chirik, P. J. High-Activity Cobalt Catalysts for Alkene Hydroboration with Electronically Responsive Terpyridine and α -Diimine Ligands. *ACS Catal.* **2015**, *5*, 622–626.

(3) Yuwen, J.; Chakraborty, S.; Brennessel, W. W.; Jones, W. D. Additive-Free Cobalt-Catalyzed Hydrogenation of Esters to Alcohols. *ACS Catal.* **2017**, *7*, 3735–3740.

(4) (a) Zhang, G.; Vasudevan, K. V.; Scott, B. L.; Hanson, S. K. Understanding the Mechanisms of Cobalt-Catalyzed Hydrogenation and Dehydrogenation Reactions. *J. Am. Chem. Soc.* **2013**, *135*, 8668–8681. (b) Obligacion, J. V.; Neely, J. M.; Yazdani, A. N.; Pappas, I.; Chirik, P. J. Cobalt Catalyzed Z-Selective Hydroboration of Terminal Alkynes and Elucidation of the Origin of Selectivity. *J. Am. Chem. Soc.* **2015**, *137*, 5855–5858. (c) Fu, S.; Chen, N.-Y.; Liu, X.; Shao, Z.; Luo, S.-P.; Liu, Q. Ligand-Controlled Cobalt-Catalyzed Transfer Hydrogenation of Alkynes: Stereodivergent Synthesis of Z- and E-Alkenes. *J. Am. Chem. Soc.* **2016**, *138*, 8588–8594. (d) Chakraborty, S.; Milstein, D. Selective Hydrogenation of Nitriles to Secondary Imines Catalyzed by an Iron Pincer Complex. *ACS Catal.* **2017**, *7*, 3968–3972. (e) Midya, S. P.; Landge, V. G.; Sahoo, M. K.; Rana, J.; Balaraman, E. Cobalt-Catalyzed Acceptorless Dehydrogenative Coupling of Aminoalcohols with Alcohols: Direct Access to Pyrrole, Pyridine and Pyrazine Derivatives. *Chem. Commun.* **2018**, *54*, 90–93.

(5) (a) Sauer, D. C.; Wade, H.; Gade, L. H. Cobalt Alkyl Complexes of a New Family of Chiral 1,3-Bis(2-Pyridylimino)-Isoindolates and Their Application in Asymmetric Hydrosilylation. *Inorg. Chem.* **2012**, *51*, 12948–12958. (b) Obligacion, J. V.; Chirik, P. J. Bis(Imino)Pyridine Cobalt-Catalyzed Alkene Isomerization-Hydroboration: A Strategy for Remote Hydrofunctionalization with Terminal Selectivity. *J. Am. Chem. Soc.* **2013**, *135*, 19107–19110. (c) Zhang, L.; Zuo, Z.; Leng, X.; Huang, Z. A Cobalt-Catalyzed Alkene Hydroboration with Pinacolborane. *Angew. Chem., Int. Ed.* **2014**, *53*, 2696–2700. (d) Teo, W. J.; Wang, C.; Tan, Y. W.; Ge, S. Cobalt-Catalyzed Z-Selective Hydrosilylation of Terminal Alkynes. *Angew. Chem.* **2017**, *129*, 4392–4396.

(6) (a) Semproni, S. P.; Hojilla Atienza, C. C.; Chirik, P. J. Oxidative Addition and C-H Activation Chemistry with a PNP Pincer-Ligated Cobalt Complex. *Chem. Sci.* **2014**, *5*, 1956–1960. (b) Deibl, N.; Kempe, R. General and Mild Cobalt-Catalyzed C-Alkylation of Unactivated Amides and Esters with Alcohols. *J. Am. Chem. Soc.* **2016**, *138*, 10786–10789. (c) Ren, H.; Zhou, Y. P.; Bai, Y.; Cui, C.; Driess, M. Cobalt-Catalyzed Regioselective Borylation of Arenes: N-Heterocyclic Silylene as an Electron Donor in the Metal-Mediated Activation of C-H Bonds. *Chem. - Eur. J.* **2017**, *23*, 5663–5667.

(7) (a) Mukherjee, A.; Milstein, D. Homogeneous Catalysis by Cobalt and Manganese Pincer Complexes. *ACS Catal.* **2018**, *8*, 11435–11469. (b) Junge, K.; Papa, V.; Beller, M. Cobalt-Pincer Complexes in Catalysis. *Chem. - Eur. J.* **2019**, *25*, 122–143.

(8) (a) Gibson, V. C.; Humphries, M. J.; Tellmann, K. P.; Wass, D. F.; White, A. J. P.; Williams, D. J. The Nature of the Active Species in Bis(Imino)Pyridyl Cobalt Ethylene Polymerisation Catalysts. *Chem. Commun.* **2001**, 2252–2253. (b) Zhang, G.; Scott, B. L.; Hanson, S. K. Mild and Homogeneous Cobalt-Catalyzed Hydrogenation of C = C, C = O, and C = N Bonds. *Angew. Chem.* **2012**, *124*, 12268–12272. (c) Zhang, G.; Hanson, S. K. Cobalt-Catalyzed Transfer Hydrogenation of C = O and C = N Bonds. *Chem. Commun.* **2013**, *49*, 10151–10153. (d) Du, J.; Wang, L.; Xie, M.; Deng, L. A Two-Coordinate Cobalt(II) Imido Complex with NHC Ligation: Synthesis, Structure, and Reactivity. *Angew. Chem., Int. Ed.* **2015**, *54*, 12640–12644. (e) Pang, M.; Wu, C.; Zhuang, X.; Zhang, F.; Su, M.; Tong, Q.; Tung, C.-H.; Wang, W. Addition of a B-H Bond across an Amido-Cobalt Bond: Co(II)-Catalyzed Hydroboration of Olefins. *Organometallics* **2018**, *37*, 1462–1467.

(9) (a) Davis, B. R.; Payne, N. C.; Ibers, J. A. Bonding of Molecular Nitrogen. I. Crystal and Molecular Structure of Hydridodinitrogen-tris-(Triphenylphosphine) Cobalt(I). *Inorg. Chem.* **1969**, *8*, 2719–2728. (b) Haumann, M.; Meijboom, R.; Moss, J. R.; Roodt, A. Synthesis, Crystal Structure and Hydroformylation Activity of Triphenylphosphite Modified Cobalt Catalysts. *Dalton Trans.* **2004**, No. 11, 1679–1686. (c) Mock, M. T.; Potter, R. G.; O'Hagan, M. J.;

Camaioni, D. M.; Dougherty, W. G.; Kassel, W. S.; DuBois, D. L. Synthesis and Hydride Transfer Reactions of Cobalt and Nickel Hydride Complexes to BX₃ Compounds. *Inorg. Chem.* **2011**, *50*, 11914–11928. (d) Tokmic, K.; Markus, C. R.; Zhu, L.; Fout, A. R. Well-Defined Cobalt(I) Dihydrogen Catalyst: Experimental Evidence for a Co(I)/Co(III) Redox Process in Olefin Hydrogenation. *J. Am. Chem. Soc.* **2016**, *138*, 11907–11913. (e) Friedfeld, M. R.; Shevlin, M.; Margulieux, G. W.; Campeau, L.-C.; Chirik, P. J. Cobalt-Catalyzed Enantioselective Hydrogenation of Minimally Functionalized Alkenes: Isotopic Labeling Provides Insight into the Origin of Stereoselectivity and Alkene Insertion Preferences. *J. Am. Chem. Soc.* **2016**, *138*, 3314–3324. (f) Liu, Y.; Du, J.; Deng, L. Synthesis, Structure, and Reactivity of Low-Spin Cobalt(II) Imido Complexes [(Me₃P)₃Co(NAr)]. *Inorg. Chem.* **2017**, *56*, 8278–8286. (g) Yu, S.; Wu, C.; Ge, S. Cobalt-Catalyzed Asymmetric Hydroboration/Cyclization of 1,6-Enynes with Pinacolborane. *J. Am. Chem. Soc.* **2017**, *139*, 6526–6529. (h) Klein, H.-F.; Karsch, H. H. Methylcobaltverbindungen Mit Nicht Chelatisierenden Liganden, III: Dimethyltris (Trimethylphosphin)Kobalt(II) Und Seine Derivate. *Chem. Ber.* **1976**, *109* (4), 1453–1464. (i) Bianchini, C.; Innocenti, P.; Meli, A.; Peruzzini, M.; Zanobini, F.; Zanello, P. Reactions of the Trigonal-Bipyramidal Cobalt(I) Hydride [P(CH₂CH₂PPh₂)₃-CoH] with 1-Alkynes. Synthesis and Reactivity of Acetylide, Alkenyl, and Vinylidene Complexes. *Organometallics* **1990**, *9*, 2514–2522. (j) Barton, R. J.; Holah, D. G.; Shengzhi, H.; Hughes, A. N.; Khan, S. I.; Robertson, B. E. Synthesis, Properties, and Structure of Hydrido(Cyanotrihydroborato)Tris(Triphenylphosphine)Cobalt(II). *Inorg. Chem.* **1984**, *23*, 2391–2395.

(10) (a) Ding, K.; Brennessel, W. W.; Holland, P. L. Three-Coordinate and Four-Coordinate Cobalt Hydride Complexes That React with Dinitrogen. *J. Am. Chem. Soc.* **2009**, *131*, 10804–10805. (b) Wu, S.; Li, X.; Xiong, Z.; Xu, W.; Lu, Y.; Sun, H. Synthesis and Reactivity of Silyl Iron, Cobalt, and Nickel Complexes Bearing a [PSiP]-Pincer Ligand via Si-H Bond Activation. *Organometallics* **2013**, *32*, 3227–3237. (c) Kuriyama, S.; Arashiba, K.; Tanaka, H.; Matsuo, Y.; Nakajima, K.; Yoshizawa, K.; Nishibayashi, Y. Direct Transformation of Molecular Dinitrogen into Ammonia Catalyzed by Cobalt Dinitrogen Complexes Bearing Anionic PNP Pincer Ligands. *Angew. Chem., Int. Ed.* **2016**, *55*, 14291–14295. (d) Guard, L. M.; Hebden, T. J.; Linn, D. E.; Heinekey, D. M. Pincer-Supported Carbonyl Complexes of Cobalt(I). *Organometallics* **2017**, *36*, 3104–3109.

(11) Krishnan, V. M.; Arman, H. D.; Tonzetich, Z. J. Preparation and Reactivity of a Square-Planar PNP Cobalt(II)-hydrido Complex: Isolation of the First {Co-NO}⁸-hydride. *Dalton Trans.* **2018**, *47*, 1435–1441.

(12) (a) Lin, T.-P.; Peters, J. C. Boryl-Mediated Reversible H₂ Activation at Cobalt: Catalytic Hydrogenation, Dehydrogenation, and Transfer Hydrogenation. *J. Am. Chem. Soc.* **2013**, *135*, 15310–15313. (b) Khaskin, E.; Diskin-Posner, Y.; Weiner, L.; Leitun, G.; Milstein, D. Formal Loss of an H Radical by a Cobalt Complex via Metal-ligand Cooperation. *Chem. Commun.* **2013**, *49*, 2771. (c) Ibrahim, A. D.; Tokmic, K.; Brennan, M. R.; Kim, D.; Matson, E. M.; Nilges, M. J.; Bertke, J. A.; Fout, A. R. Monoanionic Bis(Carbene) Pincer Complexes Featuring Cobalt(I-III) Oxidation States. *Dalton Trans.* **2016**, *45*, 9805–9811. (d) Camp, C.; Naested, L. C. E.; Severin, K.; Arnold, J. N-N Bond Cleavage in a Nitrous Oxide-NHC Adduct Promoted by a PNP Pincer Cobalt(I) Complex. *Polyhedron* **2016**, *103*, 157–163. (e) Sun, J.; Luo, L.; Luo, Y.; Deng, L. An NHC-Silyl-NHC Pincer Ligand for the Oxidative Addition of C-H, N-H, and O-H Bonds to Cobalt(I) Complexes. *Angew. Chem., Int. Ed.* **2017**, *56*, 2720–2724. (f) Sung, S.; Wang, Q.; Krämer, T.; Young, R. D. Synthesis and Reactivity of a PC_{Carbene}P Cobalt(I) Complex: The Missing Link in the Cobalt PXP Pincer Series (X = B, C, N). *Chem. Sci.* **2018**, *9*, 8234–8241.

(13) (a) Ingleson, M.; Fan, H.; Pink, M.; Tomaszewski, J.; Caulton, K. G. Three-Coordinate Co(I) Provides Access to Unsaturated Dihydrido-Co(III) and Seven-Coordinate Co(V). *J. Am. Chem. Soc.* **2006**, *128*, 1804–1805. (b) Ingleson, M. J.; Pink, M.; Fan, H.;

Caulton, K. G. Exploring the Reactivity of Four-Coordinate PNP₂CoX with Access to Three-Coordinate Spin Triplet PNP₂Co. *Inorg. Chem.* **2007**, *46*, 10321–10334. (c) Ingleson, M. J.; Pink, M.; Fan, H.; Caulton, K. G. Redox Chemistry of the Triplet Complex (PNP)₂Co. *J. Am. Chem. Soc.* **2008**, *130*, 4262–4276.

(14) (a) Gröger, N.; Wadepohl, H.; Gade, L. H. Iridium Complexes Containing a PNP Pincer Ligand: Syntheses, Structural Chemistry, and Bond Activations. *Eur. J. Inorg. Chem.* **2013**, *2013*, 5358–5365. (b) Gröger, N.; Rodríguez, L. L.; Wadepohl, H.; Gade, L. H. Achiral and Chiral PNP-Pincer Ligands with a Carbazole Backbone: Coordination Chemistry with d⁸ Transition Metals. *Inorg. Chem.* **2013**, *52*, 2050–2059. (c) Plundrich, G. T.; Wadepohl, H.; Gade, L. H. Synthesis and Reactivity of Group 4 Metal Benzyl Complexes Supported by Carbazole-Based PNP Pincer Ligands. *Inorg. Chem.* **2016**, *55*, 353–365. (d) Plundrich, G. T.; Wadepohl, H.; Clot, E.; Gade, L. H. η^6 -Arene-Zirconium-PNP-Pincer Complexes: Mechanism of Their Hydrogenolytic Formation and Their Reactivity as Zirconium(II) Synthons. *Chem. - Eur. J.* **2016**, *22*, 9283–9292. (e) Merz, L. S.; Wadepohl, H.; Clot, E.; Gade, L. H. Dehydrogenative Coupling of 4-Substituted Pyridines Mediated by a Zirconium(II) Synthone: Reaction Pathways and Dead Ends. *Chem. Sci.* **2018**, *9*, 5223–5232. (f) Ott, J. C.; Wadepohl, H.; Enders, M.; Gade, L. H. Taking Solution Proton NMR to Its Extreme: Prediction and Detection of a Hydride Resonance in an Intermediate-Spin Iron Complex. *J. Am. Chem. Soc.* **2018**, *140*, 17413–17417.

(15) Ott, J. C.; Blasius, C. K.; Wadepohl, H.; Gade, L. H. Synthesis, Characterization, and Reactivity of a High-Spin Iron(II) Hydrido Complex Supported by a PNP Pincer Ligand and Its Application as a Homogenous Catalyst for the Hydrogenation of Alkenes. *Inorg. Chem.* **2018**, *57*, 3183–3191.

(16) Higuchi, J.; Kuriyama, S.; Eizawa, A.; Arashiba, K.; Nakajima, K.; Nishibayashi, Y. Preparation and Reactivity of Iron Complexes Bearing Anionic Carbazole-Based PNP-Type Pincer Ligands toward Catalytic Nitrogen Fixation. *Dalton Trans.* **2018**, *47*, 1117–1121.

(17) (a) Kruck, M.; Sauer, D. C.; Enders, M.; Wadepohl, H.; Gade, L. H. Bis(2-Pyridylimino)Isoindolato Iron(II) and Cobalt(II) Complexes: Structural Chemistry and Paramagnetic NMR Spectroscopy. *Dalton Trans.* **2011**, *40*, 10406–10415. (b) Sauer, D. C.; Kruck, M.; Wadepohl, H.; Enders, M.; Gade, L. H. Spin Density Distribution in Iron(II) and Cobalt(II) Alkyl Complexes Containing 1,3-Bis(2-Pyridylimino)Isoindolate Ligands. *Organometallics* **2013**, *32*, 885–892.

(18) Evans, D. F. The Determination of the Paramagnetic Susceptibility of Substances in Solution by Nuclear Magnetic Resonance. *J. Chem. Soc.* **1959**, 2003–2005.

(19) Fryzuk, M. D.; Leznoff, D. B.; Thompson, R. C.; Rettig, S. J. One-Electron Transformations of Paramagnetic Cobalt Complexes. Synthesis and Structure of Cobalt(II) Amidodiphosphine Halide and Alkyl Complexes and Their Reaction with Alkyl Halides. *J. Am. Chem. Soc.* **1998**, *120*, 10126–10135.

(20) A low-spin configuration for the ^{ipr}(C_{bz}PNP)CoH complex is supported by DFT calculations, which revealed the low-spin configuration of 3^{ipr}-CoH to be 18 kcal/mol more stable than the high-spin analogue.^{10c,23a}

(21) Zhu, D.; Janssen, F. F. B. J.; Budzelaar, P. H. M. (Py)₂Co(CH₂SiMe₃)₂ As an Easily Accessible Source of “CoR₂”. *Organometallics* **2010**, *29*, 1897–1908.

(22) (a) Hartmann, D.; Wadepohl, H.; Gade, L. H. Synthesis and Structural Characterization of Group 10 Metal Complexes Bearing an Amidodiphosphine Pincer Ligand. *Z. Anorg. Allg. Chem.* **2018**, *644*, 1011–1017. (b) Ahn, J. M.; Peters, J. C.; Fu, G. C. Design of a Photoredox Catalyst That Enables the Direct Synthesis of Carbamate-Protected Primary Amines via Photoinduced, Copper-Catalyzed N-Alkylation Reactions of Unactivated Secondary Halides. *J. Am. Chem. Soc.* **2017**, *139*, 18101–18106.

(23) (a) Hebden, T. J.; St. John, A. J.; Gusev, D. G.; Kaminsky, W.; Goldberg, K. I.; Heinekey, D. M. Preparation of a Dihydrogen Complex of Cobalt. *Angew. Chem., Int. Ed.* **2011**, *50*, 1873–1876. (b) Murphy, L. J.; Ruddy, A. J.; McDonald, R.; Ferguson, M. J.;

Turculet, L. Activation of Molecular Hydrogen and Oxygen by PSiP Complexes of Cobalt. *Eur. J. Inorg. Chem.* **2018**, 4481–4493.

(24) (a) Vélez, C. L.; Markwick, P. R. L.; Holland, R. L.; DiPasquale, A. G.; Rheingold, A. L.; O'Connor, J. M. Cobalt 1,3-Diisopropyl-1H-Imidazol-2-ylidene Complexes: Synthesis, Solid-State Structures, and Quantum Chemistry Calculations. *Organometallics* **2010**, *29*, 6695–6702. (b) Wenz, J.; Kochan, A.; Wadepohl, H.; Gade, L. H. A Readily Accessible Chiral NNN Pincer Ligand with a Pyrrole Backbone and Its Ni(II) Chemistry: Syntheses, Structural Chemistry, and Bond Activations. *Inorg. Chem.* **2017**, *56*, 3631–3643.

(25) Suess, D. L. M.; Tsay, C.; Peters, J. C. Dihydrogen Binding to Isostructural S = 1/2 and S = 0 Cobalt Complexes. *J. Am. Chem. Soc.* **2012**, *134*, 14158–14164.

(26) The discrimination between the complexes 6^{fbu}-CoH₂ and 6^{fbu}-Co(H)₂ using NMR relaxation times was impossible as 6^{fbu}-Co(H)₂ stands in equilibrium with the paramagnetic 4^{fbu}-Co^I complex, which does not allow a reliable measurement of relaxation times.^{23b}

(27) Roy, L.; Al-Afyouni, M. H.; DeRoshia, D. E.; Mondal, B.; DiMucci, I. M.; Lancaster, K. M.; Shearer, J.; Bill, E.; Brennessel, W. W.; Neese, F.; Ye, S.; Holland, P. L. Reduction of CO₂ by a Masked Two-Coordinate Cobalt(II) Complex and Characterization of a Proposed Oxodicobalt(II) Intermediate. *Chem. Sci.* **2019**, *10*, 918–929.

(28) Zhao, Y.; Truhlar, D. G. A New Local Density Functional for Main-Group Thermochemistry, Transition Metal Bonding, Thermochemical Kinetics, and Noncovalent Interactions. *J. Chem. Phys.* **2006**, *125*, 194101.

(29) Ditchfield, R.; Hehre, W. J.; Pople, J. A. Self-Consistent Molecular-Orbital Methods. IX. An Extended Gaussian-Type Basis for Molecular-Orbital Studies of Organic Molecules. *J. Chem. Phys.* **1971**, *54*, 724–728.

(30) Weigend, F.; Ahlrichs, R. Balanced Basis Sets of Split Valence, Triple Zeta Valence and Quadruple Zeta Valence Quality for H to Rn: Design and Assessment of Accuracy. *Phys. Chem. Chem. Phys.* **2005**, *7*, 3297.

(31) Xu, Y.; Rettenmeier, C. A.; Plundrich, G. T.; Wadepohl, H.; Enders, M.; Gade, L. H. Borane-Bridged Ruthenium Complex Bearing a PNP Ligand: Synthesis and Structural Characterization. *Organometallics* **2015**, *34*, 5113–5118.

(32) Morello, G. R.; Zhong, H.; Chirik, P. J.; Hopmann, K. H. Cobalt-Catalysed Alkene Hydrogenation: A Metallocycle Can Explain the Hydroxyl Activating Effect and the Diastereoselectivity. *Chem. Sci.* **2018**, *9*, 4977–4982.

(33) Frisch, M. J.; Trucks, G. W.; Schlegel, H. B.; Scuseria, G. E.; Robb, M. A.; Cheeseman, J. R.; Scalmani, G.; Barone, V.; Mennucci, B.; Petersson, G. A.; Nakatsuji, H.; Caricato, M.; Li, X.; Hratchian, H. P.; Izmaylov, A. F.; Bloino, J.; Zheng, G.; Sonnenberg, J. L.; Hada, M.; Ehara, M.; Toyota, K.; Fukuda, R.; Hasegawa, J.; Ishida, M.; Nakajima, T.; Honda, Y.; Kitao, O.; Nakai, H.; Vreven, T.; Montgomery, J. A., Jr.; Peralta, J. E.; Ogliaro, F.; Bearpark, M.; Heyd, J. J.; Brothers, E.; Kudin, K. N.; Staroverov, V. N.; Keith, T.; Kobayashi, R.; Normand, J.; Raghavachari, K.; Rendell, A.; Burant, J. C.; Iyengar, S. S.; Tomasi, J.; Cossi, M.; Rega, N.; Millam, J. M.; Klene, M.; Knox, J. E.; Cross, J. B.; Bakken, V.; Adamo, C.; Jaramillo, J.; Gomperts, R.; Stratmann, R. E.; Yazyev, O.; Austin, A. J.; Cammi, R.; Pomelli, C.; Ochterski, J. W.; Martin, R. L.; Morokuma, K.; Zakrzewski, V. G.; Voth, G. A.; Salvador, P.; Dannenberg, J. J.; Dapprich, S.; Daniels, A. D.; Farkas, O.; Foresman, J. B.; Ortiz, J. V.; Cioslowski, J.; Fox, D. J. *Gaussian 09*, Revision D.01; Gaussian, Inc.: Wallingford CT, 2013.

(34) Kruck, M.; Wadepohl, H.; Enders, M.; Gade, L. H. Giant Residual Dipolar ¹³C-¹H Couplings in High-Spin Organoiron Complexes: Elucidation of Their Structures in Solution by ¹³C NMR Spectroscopy. *Chem. - Eur. J.* **2013**, *19*, 1599–1606.

(35) (a) Lee, C.; Yang, W.; Parr, R. G. Development of the Colle-Salvetti Correlation-Energy Formula into a Functional of the Electron Density. *Phys. Rev. B: Condens. Matter Mater. Phys.* **1988**, *37*, 785–789. (b) Becke, A. D. Density-functional Thermochemistry. III. The Role of Exact Exchange. *J. Chem. Phys.* **1993**, *98*, 5648–5652.

(36) Adamo, C.; Barone, V. Toward Reliable Density Functional Methods without Adjustable Parameters: The PBE0Model. *J. Chem. Phys.* **1999**, *110*, 6158–6170.

(37) Schäfer, A.; Horn, H.; Ahlrichs, R. Fully Optimized Contracted Gaussian Basis Sets for Atoms Li to Kr. *J. Chem. Phys.* **1992**, *97*, 2571–2577.

(38) Tomasi, J.; Mennucci, B.; Cammi, R. Quantum Mechanical Continuum Solvation Models. *Chem. Rev.* **2005**, *105*, 2999–3094.

(39) Ribeiro, R. F.; Marenich, A. V.; Cramer, C. J.; Truhlar, D. G. Use of Solution-Phase Vibrational Frequencies in Continuum Models for the Free Energy of Solvation. *J. Phys. Chem. B* **2011**, *115*, 14556–14562.

(40) Funes-Ardoiz, I.; Paton, R. S. *GoodVibes: version 2.0.3*; Zenodo, 2018; DOI: [10.5281/zenodo.1435820](https://doi.org/10.5281/zenodo.1435820).